Since January 2020 Elsevier has created a COVID-19 resource centre with free information in English and Mandarin on the novel coronavirus COVID-19. The COVID-19 resource centre is hosted on Elsevier Connect, the company's public news and information website.

Elsevier hereby grants permission to make all its COVID-19-related research that is available on the COVID-19 resource centre - including this research content - immediately available in PubMed Central and other publicly funded repositories, such as the WHO COVID database with rights for unrestricted research re-use and analyses in any form or by any means with acknowledgement of the original source. These permissions are granted for free by Elsevier for as long as the COVID-19 resource centre remains active.

Environmental Research 193 (2021) 110514

Contents lists available at ScienceDirect

Environmental Research

journal homepage: www.elsevier.com/locate/envres

Revisiting the levels of Aerosol Optical Depth in south-southeast Asia, Europe and USA amid the COVID-19 pandemic using satellite observations

Prasenjit Acharya [a,*], Gunadhar Barik [a], Bijoy Krishna Gayen [b], Somnath Bar [c], Arabinda Maiti [a], Ashis Sarkar [a], Surajit Ghosh [d], Sikhendra Kisor De [e], S. Sreekesh [f]

[a] Department of Geography, Vidyasagar University, Midnapore, West Bengal, India
[b] Department of Remote Sensing and GIS, Vidyasagar University, Midnapore, West Bengal, India
[c] Department of Geoinformatics, Central University of Jharkhand, Ranchi, India
[d] International Water Management Institute (IWMI), Sri Lanka
[e] Geological Survey of India, Kolkata, India
[f] Center for the Study of Regional Development, Jawaharlal Nehru University, New Delhi, India

ARTICLE INFO

Keywords:
COVID-19
AOD
NO_2
SO_2
MODIS
OMI

ABSTRACT

The countries around the world are dealing with air quality issues for decades due to their mode of production and energy usages. The outbreak of COVID-19 as a pandemic and consequent global economic shutdown, for the first time, provided a base for the real-time experiment of the effect of reduced emissions across the globe in abetting the air pollution issue. The present study dealt with the changes in Aerosol Optical Depth (AOD), a marker of air pollution, because of global economic shutdown due to the coronavirus pandemic. The study considered the countries in south and south-east Asia (SSEA), Europe and the USA for their extended period of lockdown due to coronavirus pandemic. Daily Aerosol Optical Depth (AOD) from Moderate-resolution imaging spectroradiometer (MODIS) and tropospheric column density of NO_2 and SO_2 from Ozone monitoring instrument (OMI) sensors, including meteorological data such as wind speed (WS) and relative humidity (RH) were analyzed during the pre-lockdown (2017–2019) and lockdown periods (2020). The average AOD, NO_2 and SO_2 during the lockdown period were statistically compared with their pre-lockdown average using Wilcoxon-signed-paired-rank test. The accuracy of the MODIS-derived AOD, including the changing pattern of AOD due to lockdown was estimated using AERONET data. The weekly anomaly of AOD, NO_2 and SO_2 was used for analyzing the space-time variation of aerosol load as restrictions were imposed by the concerned countries at the different points of time. Additionally, a random forest-based regression (RF) model was used to examine the effects of meteorological and emission parameters on the spatial variation of AOD. A significant reduction of AOD (−20%) was obtained for majority of the areas in SSEA, Europe and USA during the lockdown period. Yet, the clusters of increased AOD (30–60%) was obtained in the south-east part of SSEA, the western part of Europe and US regions. NO_2 reductions were measured up to 20–40%, while SO_2 emission increased up to 30% for a majority of areas in these regions. A notable space-time variation was observed in weekly anomaly. We found the evidence of the formation of new particles for causing high AOD under high RH and low WS, aided by the downward vertical wind flow. The RF model showed a distinguishable relative importance of emission and meteorological factors among these regions to account for the spatial variability of AOD. Our findings suggest that the continued lockdown might provide a temporary solution to air pollution; however, to combat persistent air quality issues, it needs switching over to the cleaner mode of production and energy. The findings of this study, thus, advocated for alternative energy policy at the global scale.

1. Introduction

The spreading of the coronavirus, a genus of the severe acute respiratory syndrome (SARS)-Cov-2, throughout the world by human transmission has turned it into a global pandemic. On March 11, 2020, the World Health Organization (WHO) announced the COVID-19 disease

* Corresponding author.
E-mail addresses: prasenjit.ac@gmail.com, prasenjit.ac@mail.vidyasagar.ac.in (P. Acharya).

https://doi.org/10.1016/j.envres.2020.110514
Received 22 August 2020; Received in revised form 29 October 2020; Accepted 18 November 2020
Available online 25 November 2020
0013-9351/© 2020 Elsevier Inc. All rights reserved.

caused by the coronavirus-as global pandemic (https://www.who.int/dg/speeches) when the spread of the virus had infected 118,000 population of 114 countries. The countries around the world were advised to contain the spread of the virus by putting measures as suggested by WHO (WHO, 2020). Consequently, the majority of the countries in the world where COVID-19 disease outbreak happened at a noticeable level or expected to climb up soon decided to impose complete nationwide lockdown, which resulted in stopping most of the economic activities and restricting the movement of the people to combat the spread of coronavirus. With economies in standby mode, a significant reduction in emission was expected that could reduce the pollution level, especially, the aerosol load in the atmosphere and corresponding reduction of the Aerosol Optical Depth (AOD) – a measure of extinction of light energy in visible channel due to aerosol's scattering and absorption - at the global scale.

Several recent studies carried out on the outbreak of COVID-19 aiming to study the improvement in the air quality index (AQI) due to the reduction of emission (Mahato et al., 2020; Sharma et al., 2020; Tobías et al., 2020; Chauhan and Singh, 2020). A significant reduction in the $PM_{2.5}$ was observed over Malaysia (Abdullah et al., 2020), China (Bao and Zhang, 2020; Li et al., 2020), India (Sharma et al., 2020), Spain (Tobias et al., 2020), and over Brazil (Dantas et al., 2020). Collivignarelli et al. (2020) reported that the restriction in people's movement and social distancing measure has significantly reduced $PM_{2.5}$, PM_{10}, BC, CO and NO_x level in the city of Milan in Italy. However, their study noted a significant improvement of surface O_3 that they attributed to the reduction of NO_x and intense solar radiation. Kanniah et al. (2020) reported up to 32% reduction in particulate matter in Malaysia due to imposition of lockdown. Additionally, the study found up to 64% reduction in NO_2, while 9–20% reduction in SO_2 and 25–31% reduction in CO was estimated from ozone monitoring instrument (OMI) onboard Aura satellite. Over Sao Paolo in Brazil, Nakada and Urban (2020) demonstrated more than 54% reduction in NO_x, and up to 64% reduction in CO during the lockdown period. The estimation over eastern China showed a 50% reduction of NO_x emission due to restriction in the movement to contain the spread of the coronavirus (Zhang et al., 2020). The study in the city of Tehran in Iran in the middle east, also demonstrated a notable reduction of NO_2 and SO_2, while O_3 and $PM_{2.5}$ levels increased during lockdown period (Broomandi et al., 2020). Wang et al. (2020) reported the reduction of $PM_{2.5}$ was not as per expectation despite near-complete lockdown. The study also reported that the unfavorable meteorology often overwhelmed the lockdown effect. A similar finding was reported by Li et al. (2020) considering the pollution source contribution function.

With nearly 15% contribution from anthropogenic sources to the total aerosol load, $PM_{2.5}$ plays a vital role in the global environment and health (Klimont et al., 2017). The study also showed a regional-scale analysis of the emission of primary anthropogenic aerosols that witnessed a decrease of emission in high-income group countries, while middle- and low-income group countries were still having a higher contribution to the total global emission of $PM_{2.5}$ (Klimont et al., 2017). Cohen et al. (2017) reported an annual average concentration of $PM_{2.5}$ more than 50 μg m^{-3} for India, China, Pakistan, and Afghanistan in SSEA, while it was less than 15 μg m^{-3} for Europe and the USA. The estimates at the global level from the Emission Database for Global Atmospheric Research (EDGAR), for the year 2012, showed the total emissions of NO_2 and SO_2 were about 3933 and 4493 Mt annually (Crippa et al., 2020; Fioletov et al., 2016). The emission database considered all sectors of anthropogenic activities as recognized by the IPCC. The database recognizes, transport sector as one of the prime sources of NO_2 emission while burning fossil fuel and biofuel to produce energy in the power plant is one of the principal sources of SO_2 emission in the atmosphere. The emission database (for the year 2012), however, noticed a wide-scale regional variation. The level of NO_2 and SO_2 emissions in the US was computed as 551 and 225 Mt y^{-1}, respectively, mostly coming from the public transport and industrial sectors (L. L. He et al., 2020; M. Z. M.Z. He et al., 2020). The Eurozone constitutes about 571 and 782 Mt y^{-1} of NO_2 and SO_2 emissions, while for SSEA, these emission estimates were 900 and 1267 Mt y^{-1}, respectively. The quantity of such an emission, including the primary emission of particulate matter into the atmosphere increases the AOD through photochemical reactions that transform these gaseous precursors into particulate matter (Seinfeld and Pandis, 2006). The estimates by Yoon et al. (2014) had shown that AOD reduced to 38.5% over Europe and 33% over USA from 2000 to 2009. In contrast, AOD, for the same period, over China and India had increased up to 26% and 24%, respectively. The reason for decreasing AOD over the USA and Europe was attributed to the reduced emission from industry, domestic and transport sectors by putting strong emission policy towards curbing air pollution issues (Hilboll et al., 2013; Streets et al., 2006; Yoon et al., 2012; Yoon et al., 2011; Zhao et al., 2008). On the other hand, the increasing trends over India and China were attributed to augmented levels of emissions due to increase in urban-industrial activities in association to their GDP growth (Smith et al., 2001; D. G Streets et al., 2003; Zhao et al., 2008; Smith et al., 2011; Chin et al., 2014). The evidence from these studies suggested a lower aerosol content (or AOD) in the atmosphere resulting in better AQI under the reduced scenario of anthropogenic emissions. As the AOD represents a comprehensive state of the quality of the air at any given time and space, it could be used at various spatial scales to analyze the pollution level. With a decision for nationwide shutdown due to the outbreak of COVID-19 and its consequent fatalities, all forms of industrial activities and most of the public and private transport were either slowed down or halted for more than six weeks in majority of the areas in SSEA, Europe and US regions. The reduced emission under such scenario alters the aerosol load at the continental scale. The studies, mentioned before in this regard, have primarily addressed the changes of AQI at the city-scape, or the national level. As the countries around the world have faced a distinguishable impact of COVID-19, the measures to contain the spread of the virus varied widely. Thus, no single and uniform time frame is appropriate for studying the effect of lockdown measures on AQI among the affected countries. Due to such limitation, the available literature lacks a comprehensive scenario of the changes of aerosol load at the continental scale. In this work, we tried to analyze the changes in the aerosol load at the larger spatial scale using both satellite and in-situ observations, especially, over SSEA (China, India, Pakistan, Nepal, Bangladesh and other south-east Asian countries) and European region due to the mass infection and fatality of COVID-19, and consequent nationwide lockdown. The study also considered the changes of AOD over the USA for a nationwide lockdown for more than six weeks due to exceptionally high COVID-19 casualties. A comparative analysis of the change in AOD among the regions was presented considering the AOD levels in the pre-lockdown and lockdown periods. The space-time variation of NO_2 and SO_2 was also taken into consideration to explain the regional difference of AOD. Moreover, we considered the meteorological fields and the regional emission characteristic in a machine learning diagnostic framework to explain their contribution in causing spatial variation of AOD at a larger spatial scale.

2. Materials and method

2.1. Aerosol Optical Depth (AOD)

The level-3 (L3) daily AOD data at 550 nm (MOD08_D3) from MODIS - onboard Terra satellite - was used in this study (Table 1). The MOD08_D3 AOD data with collection version 6.1 (C6.1) is a gridded atmospheric product with a spatial resolution of 1° that is developed from daily level 2 aerosol product. The C6.1 uses dark target (DT) (Levy et al., 2013), deep blue (DB) (Hsu et al., 2013) algorithm for separately retrieve the aerosol optical properties over visibly dark and bright surfaces, respectively. Additionally, a combined DT and DB (DTB) algorithm that uses the criteria of normalized difference vegetation index for generating AOD dataset was also used in C6.1 (Wei et al., 2019). The

Table 1
The description of data used for the analysis.

Data	Duration	Temporal/ Spatial Resolution	Sources
NO2 Tropospheric Column (30% Cloud Screened) (OMNO2d v003) SO2 Column Amount (OMSO2e v003)	SSEA: Lockdown period- 25th January - 30th April 2020; Pre-lockdown period- 25th January - 30th April 2010-2019- Europe: Lockdown period: 6th March - 30th April 2020; Pre-lockdown period-6th March - 30th April 2010–2019 USA: Lockdown period- 22nd March - 30th April 2020; Pre-lockdown- 22nd March - 30th April 2010–2019	Daily, 0.25 ° × 0.25 °	https://disc.gsfc.nasa.gov/datasets
Aerosol Optical Depth (AOD) (MOD08 D3 v6.1)		Daily, 1 ° × 1 °	https://lpdaac.usgs.gov
Relative humidity (%)		Daily, 0.25 ° × 0.25 °	https://psl.noaa.gov/
Near surface wind speed (m/s)	SSEA: Lockdown period- 25th January - 30th April 2020; Europe: Lockdown period: 6th March - 30th April 2020; USA: Lockdown period- 22nd March - 30th April 2020	Daily, 0.25° × 0.25°	https://disc.gsfc.nasa.gov/datasets/GLADS_NOAH025_3H_2.1
Vertical wind velocity or omega at 850 hPa (Pascal/s)	During the lockdown period as mentioned above	Daily, 2.5° × 2.5°	https://psl.noaa.gov/data/gridded/data.ncep.reanalysis.pressure.html

accuracy of the MODIS derived AOD concerning with a collection of ground-based sun-photometer (SP) and Aerosol Robotic Network (AERONET) was defined to be ± (0.05 + 15%) over land (Remer et al., 2005, 2008; Levy et al., 2010).

2.2. NO_2 and SO_2 data

Daily data about vertical column density (VCD) of NO_2 and SO_2 from the OMI sensor, onboard NASA's Aura satellite, were used (Table 1). The OMI was deployed for monitoring global atmospheric Ozone and other pollutants, such as NO_2, SO_2, HCHO, BrO, and OClO, at a spatial resolution of 0.25°. For retrieving NO_2, the OMI-measured backscattered radiances within the wavelength of 270–340 nm were used for spectral fitting to the laboratory-measured absorption spectra of NO_2, H_2O and O_3 to calculate the slant column density (SCD). The SCD, after subtracting the contribution from the stratosphere is converted into tropospheric VCD by applying air mass factor (AMF) interpolated from LUT with OMI measured input parameters, such as viewing geometry, surface reflectivity, cloud pressure, cloud radiance fraction, assuming a priori NO_2 vertical profile shape (Bhartia, 2002; Li et al., 2013). For retrieving SO_2, Principal Component Analysis (PCA)-based algorithm was applied to the OMI-radiance (Li et al., 2013; Krotkov et al., 2016). Using clear sky radiances and AMF, PCA algorithm was applied over a full spectral range of 310–340 nm to detect VCD of SO_2. The OMI sensor mapped NO_2 in molecules cm^{-2}, while SO_2 expressed in the Dobson unit (DU; 1 DU = 2.69 × 1016 molecules cm^{-2}). The uncertainty of the SO_2 detection using the current algorithm is about 0.5 DU which is within the 1σ distance (Li et al., 2013). However, with time averaging of the cloud free OMI scenes, this noise reduces to 0.2 DU. The validation of OMI-derived VCD of SO_2 data using aircraft measurement further showed an error of 45–80% over a polluted region, with a correlation of 0.92 by applying the local AMF correction (Lee et al., 2009). The uncertainty in estimating the NO_2 remains within 20% for the cloud free OMI scenes (Bucsela et al., 2013; Irie et al., 2012; Lamsal et al., 2010).

2.3. Meteorological data

We used near-surface daily gridded (0.5° × 0.5°) reanalysis data of relative humidity (RH) from National Center for Environmental Prediction (NCEP), NOAA, due to their decisive role in removing the aerosol particles from the atmosphere as well as reducing the amount of gaseous precursor (Kalnay et al., 1996). The NCEP reanalysis data is produced using state-of-the-art analysis/forecast system to perform data assimilation using past data.

The near-surface wind speed (WS) during the lockdown period (Table 1) was taken from the NASA Global Land Data Assimilation System (GLADS) Version 2. The GLADS 2.1 surface meteorological data are generated using NOAH model 3.6 in the Land Information System (LIS) version 7. These meteorological data are the outcome of a combination of modeled and observational data produced at the 3-hourly interval with a spatial resolution of 0.25°. The 3-hourly WS data were aggregated into daily averages for the analysis. Furthermore, daily data of the vertical wind velocity (omega (Pascal/s)) at 850 hPa (~1.4 km above from mean sea level) from National Center for Atmospheric Research (NCAR)/NCEP was used in the analysis. This data is a derived product of Reanalysis project under the NCAR/NCEP that perform global data assimilation from observational and satellite data. A positive value of omega suggests the downward movement of the wind (↓), while a negative value suggests upward movement (↑). We also used Hybrid Single-Particle Lagrangian Integrated Trajectory (HYSPLIT) model (Draxler and Hess, 1998) from NOAA Air Resource Laboratory (ARL) website (https://www.ready.noaa.gov/HYSPLIT.php) for computing back trajectories to show long-range transportation paths of the pollutants.

2.4. AOD data from Aerosol Robotic Network (AERONET)

Daily in-situ observations of AOD at 550 nm were obtained from AERONET stations (web reference) for validating the MODIS-derived AOD and its changing pattern due to the imposition of lockdown measures. The AERONET is a type of sky radiometer that measures the columnar aerosol concentration in the direction of solar zenith angle. More than 350 AERONET stations are situated globally to facilitate aerosol studies using remotely sensed satellite images, especially, the AOD, derived from MODIS. We used the AOD data from active stations which, at least, archive AOD information on a regular basis during the pre-lockdown and lockdown periods. A sum of 13 AERONET stations – spread over the SSEA, Europe and USA – were used in this study (Table 2). The concurrent observations of AOD from the AERONET stations – at the passing time of Terra satellite that carries MODIS – were used during per-lockdown and lockdown periods. The collocated observations of AOD from MODIS pixels were used for building the validation dataset.

3. Methods

The timeline for the lockdown period due to the outbreak of COVID-

Table 2
The details of the AERONET stations selected over SSEA, Europe and over the US regions.

Continent	Country/ State	Station	Lat/Long	Elevation (In Meters)
SSEA	Thailand	Chiang Mai Met Station	18.771°N/ 98.972°E	312
		Silpakorn University	13.819°N/ 100.041°E	72
		Ubon Ratchathani	15.246°N/ 104.871°E	120
		Songkhla Met Station	7.184°N/ 100.605°E	15
Europe	France	Toulon	43.136°N/ 6.009°E	50
		Toulouse MF	43.573°N/ 1.374°E	160
		OHP Observatoire	43.935°N/ 5.710°E	680
		Palaiseau	48.712°N/ 2.215°E	156
	Spain	Burjassot	39.507°N/ 0.420°W	104
		Palencia	41.989°N/ 4.516°W	750
	Italy	Rome La Sapienza	41.902°N/ 12.516°E	75
USA	USA/ Colorado	NEON Sterling	40.462°N/ 103.029°W	1372
	USA/ Nevada	University of Nevada-Reno	39.541°N/ 119.814°W	1410

19 was not uniform across the countries. Therefore, for the convenience of analysis, the official declaration of the first lockdown by a country in SSEA and Europe was taken under consideration to define the lockdown period for controlled emission from anthropogenic activities (Supplement Table 1). It turns out, the lockdown period for SSEA region was from 25th January to April 30, 2020. For Europe, it was taken from 6th March to 30th April, while for the USA, the lockdown period was taken from 22nd March to April 30, 2020. The pre-lockdown period was considered from 2017 to 2019 in the above-mentioned specific time intervals for SSEA, Europe and the US. Daily observations of AOD from MODIS, and NO_2 and SO_2 from OMI sensors were used within these time-intervals of pre-lockdown and lockdown periods. Three years average of the input variables for defining their pre-lockdown state, as suggested by Sicard et al. (2020), was used in this study for reducing the meteorological effects.

The mean of AOD, NO_2 and SO_2 was computed from daily observations for the pre-lockdown and lockdown periods. The relative percentage difference (RPD) between pre-lockdown and lockdown was calculated based on the computed mean values (Equation (1)).

$$RPD = \left(\frac{x_l - x_{pl}}{x_{pl}}\right) \times 100 \tag{1}$$

The x_l and x_{pl} are values for the lockdown period and pre-lockdown periods. A negative RPD refers to a higher magnitude of AOD, NO_2 and SO_2 during pre-lockdown, while a positive RPD refers to a higher value of these variables during the lockdown period. The negative and positive RPDs of AOD, NO_2 and SO_2 were tested for their significant difference during pre-lockdown and lockdown periods. For this purpose, two sets of sampling points having a size of 500 each were randomly selected on the RPD images. The first sampling set was selected on the areas of positive RPD, while the second set was chosen on the negative RPD. The sampling points of each of these two sets were then used for extracting the values of AOD from time-series MODIS AOD product during the pre-lockdown and lockdown periods. The sampled values were tested for normality test using Shapiro-Wilk test with a critical value (α) 0.05 (p-value = 0.05). The test statistics revealed the distributions - for positive and negative RPDs - are not normal. Thus, the significant changes of AOD during lockdown period as compared to pre-lockdown period was tested through non-parametric Wilcoxon-signed-paired-rank test with α of 0.05.

For validating the changes of AOD, derived from MODIS, daily observations of AOD from AERONET stations were used during the pre-lockdown and lockdown periods. The observations of AOD (at 550 nm) from AERONET were obtained following the passing time of MODIS (using a buffer time of 30 min) over the corresponding AERONET stations. In addition, the collocated AOD values from MODIS pixels were extracted for the validation. Following three-step approaches – as mentioned in the earlier studies (Glantz et al., 2019; Gupta et al., 2018; Jing-Mei et al., 2010; Misra et al., 2008) - were adopted to report the accuracy of the estimated AOD from MODIS: (i) the mean absolute error (MAE) and (ii) the root-mean-square error (RMSE) between AERONET and MODIS-derived AOD data (Equations 2 - 3) and (iii) the coefficient of determination (R^2) using linear regression model. The uncertainty of the MODIS-derived AOD (τ_{MODIS}) with reference to AERONET-derived AOD ($\tau_{AERONET}$) during pre-lockdown and lockdown periods was computed using the expected error (EE) estimates (Equation (4)) given by Levy et al. (2010) and Remer et al. (2005). For quality assured collocated AOD pixels, the τ_{MODIS} ranges within the limit defined in Equation (4). As per the estimates of Remer et al. (2005) and Levy et al. (2010), this uncertainty envelope should contain 66% of the τ_{MODIS} observations - equivalent to one standard deviation under normal distribution curve – which are closely associated with good quality $\tau_{AERONET}$ observations.

$$MAE = \frac{1}{n}\sum|\tau_{AERONET} - \tau_{MODIS}| \tag{2}$$

$$RMSE = \sqrt{\frac{\sum(\tau_{AERONET} - \tau_{MODIS})^2}{n}} \tag{3}$$

Where n in equations (2) and (3) is number of observations.

$$\tau_{AERONET} - EE \leq \tau_{MODIS} \leq \tau_{AERONET} + EE \tag{4}$$

$$EE = \pm(0.05 + 0.15 \times \tau_{AERONET})$$

Further, the RPD was estimated for $\tau_{AERONET}$ in conjunction with the collocated AOD data from MODIS considering the observations from pre-lockdown and lockdown periods. As the number of observation days corresponding to lockdown and pre-lockdown periods is not same, we used contemporaneous dates to estimate the mean values of $\tau_{AERONET}$ and τ_{MODIS} during the pre-lockdown and lockdown periods.

The 8-days standard anomaly (z_x) during the lockdown period, as mentioned above, was also computed for tracking the progress of AOD, NO_2 and SO_2 dynamics in space-time context (Equation (5)).

$$z_x = \frac{x_i - \overline{x}}{\delta} \tag{5}$$

Where x_i represents an observation for the lockdown period in 2020, and $\overline{x}$ and δ are the mean and standard deviation of 8-days data from 2017 to 2019.

As the lockdown measures were not imposed at the same time for all of the concerned countries and some of the nations avoided nationwide lockdown, however, adopted appropriate social distancing measures, the zonal pattern of emission and their long-range transportation through the active wind system is essential in accounting for the regional AOD variation. Thus, we used HYSPLIT model to compute 7-days back trajectories to evaluate the effect of long-range transport on the variation of AOD.

We also used the meteorological fields such as RH and WS in combination with the NO_2 an SO_2 concentration for analyzing the spatial variation of AOD during the lockdown period. For this purpose, we used a random forest-based (RF) regression model. Due to the complexity of the statistical distribution of the input data, RF regression model was

used to simulate the effect of controlled emission of NO_2 and SO_2 due to imposition of lockdown measures, including the mesoscale variation of RH and WS, on the spatial variation of AOD. The random forest is a machine learning algorithm that uses bootstrapping and bagging approach to increase the accuracy of prediction by reducing the mean sum of square of error (MSE) (Breiman, 2001). Prior to train the model, the average of the input variables was computed from their respective daily observations for the period of lockdown. The RF model was trained on the time-averaged images of AOD, NO_2, SO_2, RH and near surface WS data during the lockdown period using a set of randomly selected sampling points (n = 2500). Alongside with these variables, the geo-location fields such as latitude and longitude were also used as covariates for accounting the spatial characteristics of emission. To test the model performance, the sample size was split into training (70%) and validation (30%) set. A random sampling procedure was used for bagging this 70% of the total sampling points for training into RF regression model. The number of trees for training the model was 100 as there was no further improvement in reduction of MSE. The performance of the model was tested using the validation set. The relative importance of the input variables was measured. Moreover, the predicted AOD at the lockdown condition and the observed AOD from MODIS were subtracted to evaluate the prediction error of the model.

4. Results

4.1. Spatio-temporal variation of AOD, NO_2, and SO_2 in pre-lockdown and lockdown periods

The mean AOD over the eastern part of SSEA that includes areas over Thailand, Laos, the northern part of Vietnam and Bangladesh, and in eastern China showed moderate to high aerosol load (AOD 0.6–0.8) during the pre-lockdown period (Fig. 1a). For the lockdown period, the mean AOD showed notable reduction (AOD $\leq$ 0.6) over eastern China though high AOD ($\geq$0.8) prevailed over Thailand, Laos, Bangladesh,

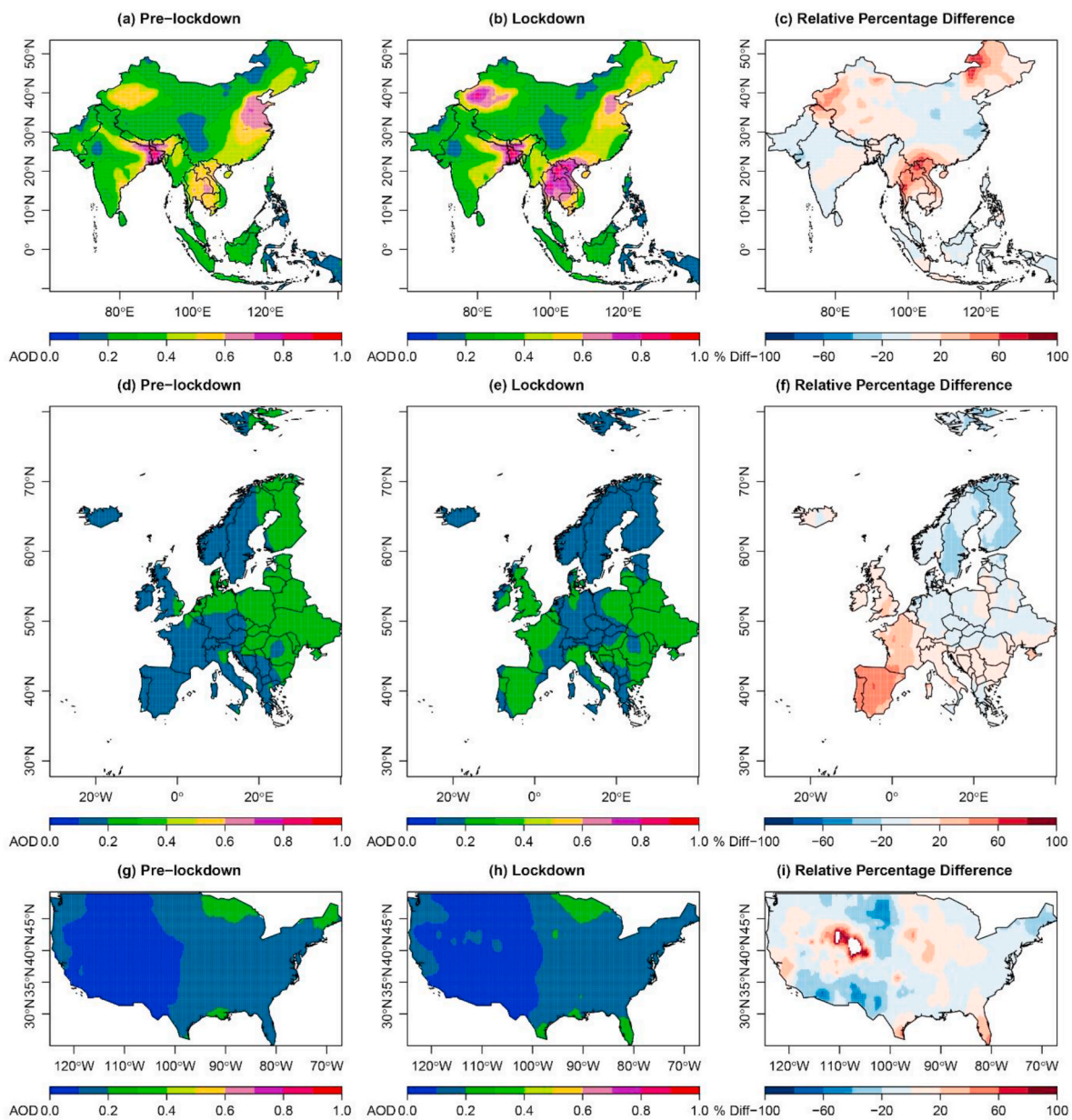

Fig. 1. The AOD levels during the lockdown and pre-lockdown periods including the percentage difference in AOD over SSEA, Europe and US. The mean of the lockdown period for SSEA was computed from 25th January to 30 April 2020, for Europe, it was from 6th March to 30th April 2020, and for US, it was from 22nd March to April 30, 2020. The mean of the pre-lockdown period was computed in these respective time intervals, but the years considered for this was 2017–2019.

northern Vietnam and eastern India (Fig. 1b). The AOD remained high over western China in the parts of Gobi Desert during the lockdown period, while it was moderate (0.4–0.6) during the pre-lockdown period. Such a high aerosol load during the lockdown period is attributed to natural dust emission, intensified by the active wind in this part of western China. The change in AOD through RPD showed a reduction up to 20% in the lockdown period over most of the central and eastern Chinese territory implying to the effectiveness of nationwide lockdown (Fig. 1c). The majority of the areas over western India, Pakistan, Malaysia, Indonesia and the Philippines also showed a reduction of 20% AOD. However, the areas over Myanmar, Thailand, Laos and Vietnam showed 30–60% enhancement of aerosol load. The enhancement in AOD was also observed over the western China and north-east Chinese territory (30–60%).

Over Europe, a majority of areas in the east showed a mean AOD within the range of 0.2–0.3, while the areas over western Europe showed a mean AOD < 0.2 during the pre-lockdown period (Fig. 1d). During the lockdown period, the AOD, for a majority of the areas in central and northern Europe, was <0.2 (Fig. 1e). At the same time, the areas over eastern and western Europe showed AOD within 0.2–0.3 during the lockdown period. Up to 20% reduction in AOD was estimated in areas over central and eastern Europe. In contrasts, the areas over western Europe such as France, Spain, and Portugal showed a 30–60% increase in AOD (Fig. 1f). The areas over Italy, Greece and other south-east European countries also showed an increase of AOD up to 20%.

The mean AOD during the pre-lockdown period over most of the regions in the eastern USA was observed around 0.1 to 0.2 (Fig. 1g). The western US, however, showed up comparatively lower mean AOD during the pre-lockdown period (AOD ≤ 0.1). The spatial pattern of mean AOD during the lockdown period stayed apparently similar to that of the pre-lockdown period (Fig. 1h). The percentage change, however, showed a 20% reduction in AOD over majority of areas in the US (Fig. 1i). The mid-western US registered relatively more reduction in AOD amounted to 20–60% during the lockdown period. In contrasts, the clusters of increased AOD (20–60%) were found in some of the areas in the western, mid-west, mid-east and coastal part of south-east US during the lockdown period. The pairwise comparison through Wilcoxon-signed-paired-rank test for all negative changes over SSEA, Europe and US show a significant reduction in AOD (Table 3). The areas of positive change also show a significant increase in AOD (Table 3).

Likewise AOD, the mean values of NO_2 during the periods of pre-lockdown and lockdown showed significant differences (Table 2), especially, over eastern China in SSEA (Fig. 2a–b). About 20–40% reduction in NO_2 was measured in eastern China, while 20–40% reduction was estimated over India and other SSEA countries (Fig. 2c). About 20–40% reduction was estimated during lockdown period for the majority of areas over Europe except for eastern and northern European countries which did not impose stricter nationwide lockdown due to relatively lower number of events of COVID-19 (Fig. 2d–f). About 20–40% reduction in NO_2 emission was estimated over most of the provinces in the US during the lockdown period (2 g – 2i). However, up to 20% increase in the NO_2 concentration was estimated in areas which are primarily clustered in southern US province. Unlike NO_2, the estimated mean SO_2 during the lockdown period exhibited relatively higher concentration in majority of the areas over central and western China, Pakistan, northern India and areas over other SSEA countries such as Thailand, Laos, Vietnam, Cambodia and Indonesia (Fig. 3a – 3c). About 10–30% increase in SO_2 was estimated in those areas during the lockdown period. However, about 10% decrease was estimated in areas over the east and north-east China, the southern part of India, Myanmar, and other SSEA regions. The percentage change of SO_2 during the lockdown period showed a 30% increase in south-east and eastern European countries. Up to 20% increase in SO_2 was also noted over France, southern Germany and Italy in mainland Europe (Fig. 3d–f). In contrasts, up to 10% decrease in SO_2 is observed during the lockdown period over a majority of the north and western European countries, including the southern part of England. Similarly, SO_2 emission over the majority of areas in the USA was increased by 10–30% during the lockdown period (Fig. 3g–i). However, up to 10% reduction in SO_2 emission was estimated in the south and the mid-western USA.

4.2. Validation of the changes of AOD

The collocated observations of AOD for the selected AERONET stations showed a MAE within 0.40–0.17 (RMSE ~ 0.06–0.25) during the pre-lockdown period, while it ranges within 0.20–0.17 (RMSE ~ 0.02–0.23) during the lockdown period (Table 4). The MAE and RMSE remained higher for the stations in SSEA region due to complexity of aerosol types and meteorological conditions, including the variation of land cover type that lead to a poor estimation of the relationship between the estimated surface reflectance at 470 nm and 660 nm given by Kaufman et al. (1997) and the measured top-of-the-atmospheric (TOA) reflectance from MODIS at the same wavelengths. Such relationship forms the basis of look-up table (LUT) inputs for AOD retrieval (Remer

Table 3
The median values of pre-lockdown and lockdown periods, and their statistical difference through non-parametric Wilcoxon-signed-paired-rank test. The median values were computed based on the values of the sampling points on the image of the relative percentage difference (RPD). A sum of 500 ($n = 500$) sampling points were selected on the pixels of negative RPD and another set of 500 sampling points were selected on the pixels of positive RPD separately.

		Negative RPD				Positive RPD			
Region		Median (Pre-lockdown)	Median (Lockdown)	Median Difference	p-value	Median (Pre-Lockdown)	Median (Lockdown)	Median Difference	p-value
	AOD	0.31	0.28	−0.03	<2.2e-16	0.33	0.40	0.07	<2.2e-16
SSEA	NO_2	0.18	0.15	−0.03	<2.2e-16	0.10	0.11	0.01	<2.2e-16
	SO_2	0.27	0.26	−0.01	<2.2e-16	0.22	0.24	0.02	<2.2e-16
	AOD	0.20	0.17	−0.03	<2.2e-16	0.18	0.21	0.03	<2.2e-16
Europe	NO_2	0.21	0.18	−0.03	<2.2e-16	0.12	0.14	0.02	<2.2e-16
	SO_2	0.33	0.31	−0.02	<2.2e-16	0.33	0.36	0.03	<2.2e-16
	AOD	0.11	0.09	−0.02	<2.2e-16	0.14	0.16	0.02	<2.2e-16
USA	NO_2	0.14	0.12	−0.02	<2.2e-16	0.13	0.14	0.01	<2.2e-16
	SO_2	0.23	0.22	−0.01	<2.2e-16	0.25	0.27	0.02	<2.2e-16

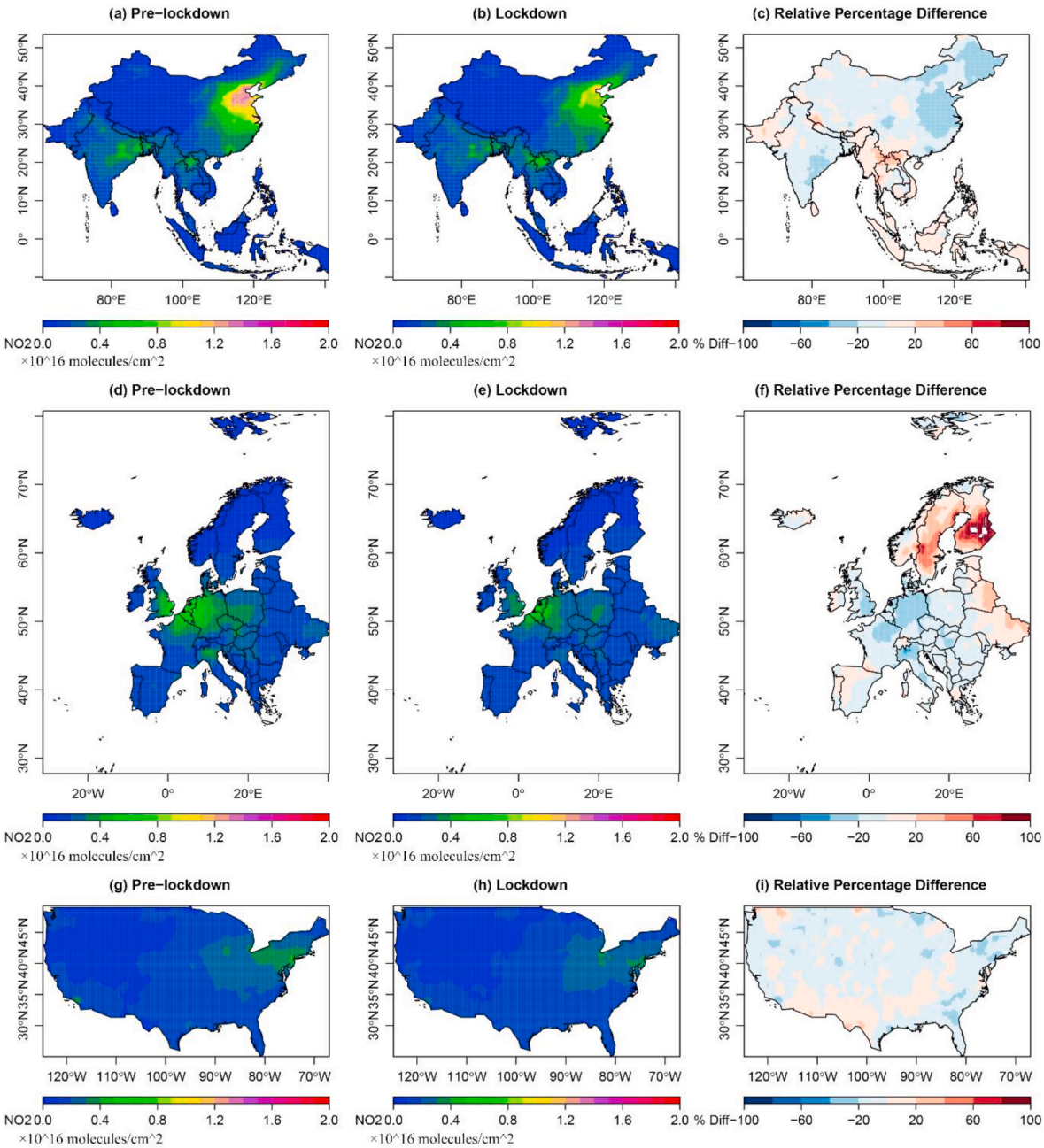

Fig. 2. NO_2 concentration (molecules/cm^2) during the lockdown and pre-lockdown periods over SSEA, Europe and the US.

et al., 2005). The EE, during the pre-lockdown period, showed more than 77% of the τ_{MODIS} observations for the stations in Europe and USA fall within EE limit that contains the high-quality MODIS observation with minimum error. Conversely, about 51% observations of τ_{MODIS} fall in EE limit for the observing stations in SSEA region during pre-lockdown period. The EE, during the lockdown period, showed more than 72% observations in that limit for the observing stations over Europe and USA, while 49% observations fall in that limit for the stations in SSEA region. The scatterplots in Fig. 4 showed a good amount of agreement at low value of AOD. As the magnitude of observed AOD ($\tau_{AERONET}$) increases, the difference between τ_{MODIS} and $\tau_{AERONET}$ increases and scatter points are falling away from the EE limit, suggesting a higher degree of uncertainty for the τ_{MODIS} observations due to the inclusion of low-quality pixel's observations. The regression coefficients (slope) for nearly all of the cases - except for the pre-lockdown period in US region - showed a magnitude equivalent to less than one, suggesting an underestimation of AOD from MODIS as compared to the AERONET. The estimated RPD values from the AERONET stations, further, showed they are in accordance with the pattern of RPD estimated from MODIS (Supplement Figure 1).

4.3. Weekly anomaly during the lockdown period

The dynamics of weekly AOD anomaly showed a large spatial extent of the negative anomaly ($z_x \sim -1.0$) in areas over the eastern part of SSEA, especially, over eastern China during third to seventh week of the lockdown (10th February – 21st March), and during the last week of lockdown (23–30th April) (Supplement Figure 2a). Within this period of lockdown, significant reductions ($z_x > -1.96$) in AOD level were measured in east and south-east China as well as over Laos, Thailand and Vietnam. Over India and Bangladesh, the spatial extent of the significant negative anomaly ($z_x > -1.96$) was found during the ninth week of

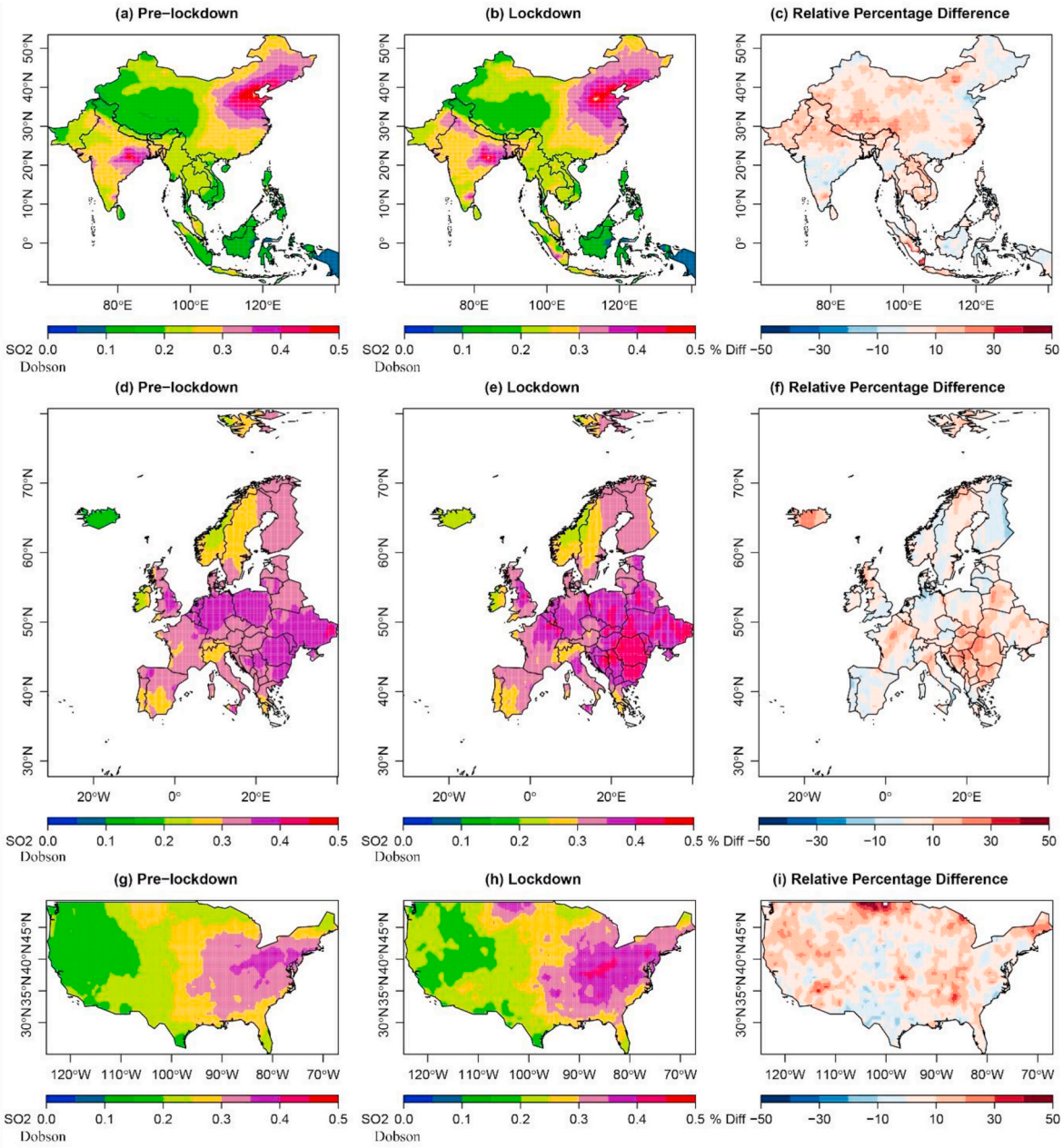

Fig. 3. The column density of SO_2 concentration (Dobson unit) during the pre-lockdown and lockdown periods over SSEA, Europe and the US.

Table 4
Details of validation measures, including the mean AOD from AERONET stations and collocated MODIS pixels during the pre-lockdown and lockdown periods. For estimating the mean AOD for the regions during the pre-lockdown and lockdown periods, the observations form AERONET stations were summed and divided by the number of observations. The mean AOD of the collocated MODIS pixels was also summarized in the same process.

Region	Period	N	Mean AOD (AERONET)	Mean AOD (MODIS)	Regression Equation	R^2	p-value	RMSE	% in EE
SEEA	Pre-Lockdown	762	0.54	0.47	y = 0.5745x+0.1591	0.59	2.48e-15	0.25	50.92
	Lockdown	132	0.58	0.60	y = 0.8339x+0.1145	0.67	5.11e-33	0.23	49.24
Europe	Pre-Lockdown	471	0.10	0.11	y = 0.7353x+0.0394	0.47	5.09e-66	0.04	81.74
	Lockdown	172	0.13	0.17	y = 0.9751x+0.0441	0.50	1.65e-27	0.09	72.67
USA	Pre-Lockdown	96	0.07	0.10	y = 1.2840x+0.0157	0.44	2.29e-13	0.06	77.08
	Lockdown	31	0.05	0.04	y = 0.6141x+0.0095	0.44	4.40e-05	0.02	100.00

lockdown (30th March – April 6, 2020). For India, such a significant reduction in AOD-level was especially obtained in the northern plain. Over Europe, AOD showed a negative anomaly ($z_x \sim -1.0$) for most of the northern and central regions during the lockdown period; however, significantly high positive anomalies ($z_x > 1.96$) were observed over western Europe that includes the areas over France, Spain, Portugal and western Germany during the second week of lockdown (14–21st March) (Supplement Figure 2b). Over the USA, a high degree of spatial variation

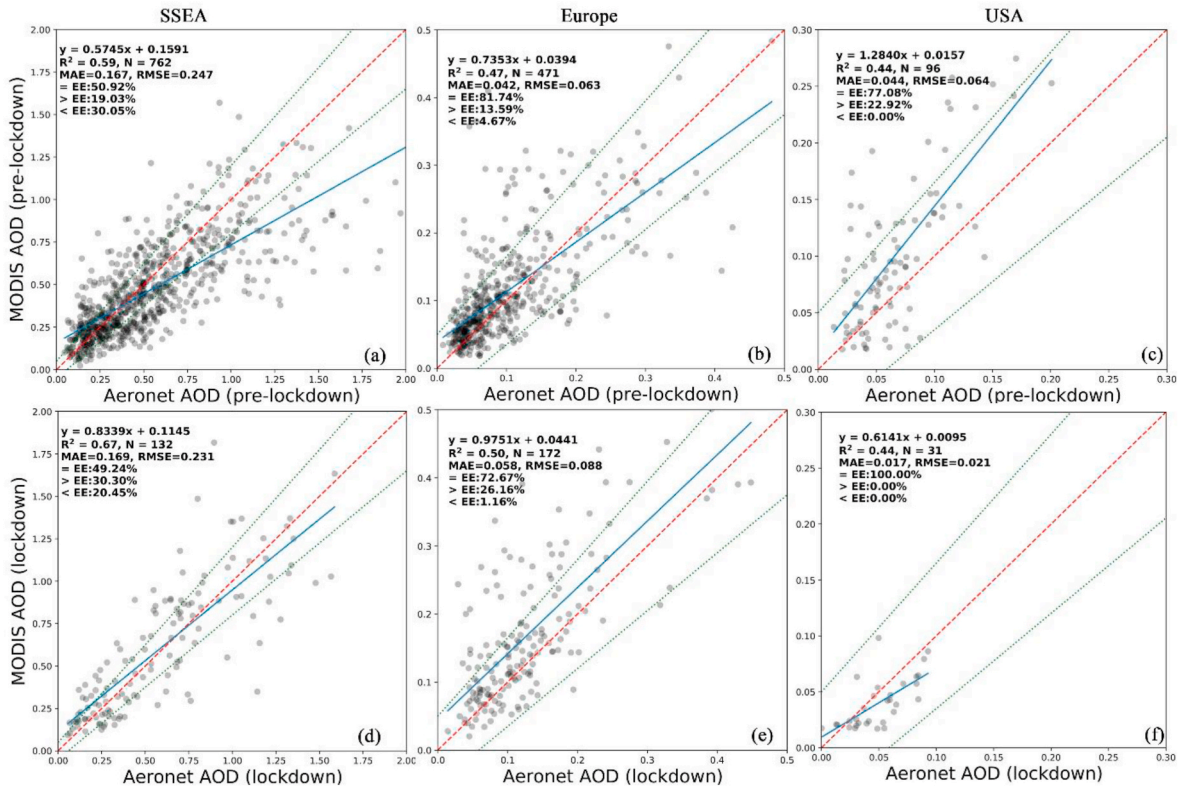

Fig. 4. Scatterplot between daily observations of AERONET and MODIS-derived AOD during (a–c) pre-lockdown and (d–f) lockdown periods. The expected error (EE) limit around the 1-1 line (dotted red line) shows uncertainty limit of the MODIS-derived AOD (τ_{MODIS}). The regression line shows the deviation from the 1-1 line implying underestimation (or overestimation) of AOD in MODIS data. The percentage of observation within the uncertainty envelope is given by = EE, while observations above the upper limit and below the lower limit are denoted by > EE and < EE, respectively. (For interpretation of the references to colour in this figure legend, the reader is referred to the Web version of this article.)

is observed in weekly AOD-anomaly, especially in central US (Supplement Figure 2c). The parts of eastern and western US show consistent negative anomaly ($z_x \sim -1.0$) from 30th March to 22nd April 2020. A cluster of the significant negative anomaly ($z_x \sim -2.0$) is observed only on the west coast during the third week (7th – 14th April) of lockdown. The positive AOD-anomaly with spatial clusters of significantly high z_x (>2.0) was observed, primarily, over the north-west and western US throughout the lockdown period, considered for this region.

The weekly progress of the NO_2 anomaly over SSEA showed an overall decrease ($z_x \sim -1.0$) for the first six weeks for majority of the areas in China. The spatial clusters of the significant negative anomaly ($z_x \sim > -1.96$) were observed in the north-eastern Chinese territory around Beijing during the first three weeks of lockdown (25th January – February 17, 2020) (Supplement Figure 3a). Towards the end of the lockdown period, considered for SSEA region, the clusters of positive anomalies ($z_x \sim 1$–3) were observed in eastern China. Over the Indian region, the spatial clusters of the significant negative anomaly were generally obtained in northern plain during the eighth through tenth week of lockdown-period (22nd March – 14th April). Among other areas in SSEA region, the clusters of consistent and significantly positive NO_2 anomaly was observed over Vietnam, Laos and Thailand. Over Europe, significant positive NO_2 anomaly was estimated for majority of the areas in the north during the first four weeks of lockdown period (Supplement Figure 3b). Much of the central and southern Europe is characterized by negative NO_2 anomaly. No significant negative anomaly with substantial spatial coverage was obtained over Europe during the period of lockdown. Over the USA, the anomaly was broadly negative; however, significant reduction in NO_2 ($z_x > -1.96$) was obtained in the south-eastern part during the first week of the lockdown period (Supplement Figure 3c). A significant increase of NO_2 ($z_x \sim 2.0$) was observed at the south of US in the fourth week of lockdown. The spatial clusters of positive NO_2 ($Z_x \sim 1$–2) anomaly were also estimated, scattered over north and south of US during the lockdown period.

The SO_2 anomaly remained mostly positive ($z_x \sim 0.5$–1.5) over the areas to the west of the SSEA region (Supplement Figure 4a). The prolific spatial clusters of high positive SO_2 anomaly were found all over the Chinese mainland during the period of lockdown. For other areas in SSEA region, such clusters of the high positive anomaly of SO_2 was observed over Pakistan, the northern part of India, and the areas over Myanmar, Thailand, Laos, Vietnam and Cambodia. Though negative anomaly of SO_2 ($z_x \sim -0.5$ to -1.0) started dominating after six weeks of lockdown, the result found no evidence of significant reduction of SO_2 during this period over the SSEA region. Over European region, the anomaly of SO_2, broadly, remained positive ($z_x > 0.5$) for the majority of areas in the north, east and south for the first four weeks of lockdown (Supplement Figure 4b). However, relatively low SO_2 concentration ($z_x \sim -0.5$) was estimated starting from the fifth week of lockdown period. A positive SO_2 anomaly with $z_x > 1.0$ was observed over the Nordic region and areas over eastern Europe towards the end of the lockdown period. The spatial clusters of high positive SO_2 anomaly were also observed for the first four weeks of imposing the lockdown measure over the US. The clusters of positive SO_2 anomaly ($z_x \sim 0.5$–1.0) were consistently observed in the eastern US for the entire period of lockdown. However, a noticeable decrease in the relative concentration of SO_2 was estimated ($z_x \sim -0.5$ to -1.0) in the north-west after the fourth week of lockdown (Supplement Figure 4c).

4.4. Random forest regression

The simulation AOD during the lockdown period through RF regression revealed the contribution of RH and NO_2 up to 38–40% in explaining the variation of the AOD in SSEA region, while WS has the

least influence in causing the spatial variation in AOD (Fig. 5a). For the European region, the WS and the NO_2 concentration explain up to 30–35% variation of AOD, while the RH and SO_2 explain up to 22–24% variation in AOD (Fig. 5b). Over the USA, the RH and WS explain up to 20–25% variation, while SO_2 and NO_2 account for up to 15–18% of the variation of AOD (Fig. 5c). It was observed that for all regions, the geolocation fields, especially, the longitude has a larger influence (>40%) in explaining the spatial variation of AOD. However, for the European region, the role of latitude field has a lesser influence (~30%) than WS in causing the spatial variation of AOD.

The degree of agreement of the predicted AOD from RF regression model using the validation AOD-dataset showed an R^2 greater than 0.94 for all three regions (Fig. 5d–f). The distribution of the magnitude of spatial error with reference to the MODIS-derived AOD showed an error-magnitude of ±0.05 for the regions of Europe and the USA (Fig. 6). In contrasts, the spatial error for the SSEA region reaches up to ±0.2 that is mostly observed as clusters in areas of high AOD in western and eastern China, the part of eastern Indian territory and Bangladesh, and in some of the areas of Thailand, Laos, Cambodia and Vietnam.

5. Discussion

Overall, the change of AOD in the SSEA, Europe and US regions due to lockdown revealed no perceivable reduction of AOD (Fig. 7). However, statistically, significant changes were obtained on the spatial clusters of negative and positive RPD (Table 3). The observation from AERONET stations across these regions – though majority of them fall under the category of positive RPD – showed a significant level of agreement with collocated MODIS-derived observations during pre-lockdown and lockdown periods (Table 4). Yet, the underestimation of τ_{MODIS} for a higher magnitude of $\tau_{AERONET}$, as found in the regression coefficients (Fig. 4), suggests significant difference of measured TOA from MODIS and AERONET due to variation of aerosol type and their absorbing property. Due to the greater variation of aerosol type and their absorbing properties, including the variation of underlying land cover in SSEA region, the TOA from MODIS remains poorly correlated with the calibrated TOA of AERONET at a given Sun-Earth distance, zenith and azimuth direction which resulting into high uncertainty and observation fall beyond the EE limit. In contrasts, TOA estimation – with reference to AERONET's measurement - is better over Europe and USA due to homogeneity of aerosol type and land cover leading to low uncertainty in estimation of AOD from MODIS. The lockdown measures substantially reduced the aerosol load in majority of the areas over SSEA, Europe and USA. However, some of the areas in these regions did not show the immediate reduction in aerosol load. Such discrepancy in the reduction of AOD is due to the non-imposition of lockdown measure by many of the countries in these regions. Moreover, the nations who went for the total shutdown, did not announce the economic standby at the same time.

The controlled emission due to lockdown measures in eastern China reduced the aerosol load significantly (Fig. 1c) though north-east and western Chinese territories exhibited a significant increase in aerosol load during the lockdown period. The reduction of NO_2 and SO_2 up to 20–30% was reported by Muhammad et al. (2020) over eastern China which was also found in this study. Such a reduction in the emission led to the overall lowering of the aerosol load over eastern China. However, the increase in AOD in the north-east Chinese territory during lockdown is attributed to major industrial activities including the emission from the thermal power plants in this area which lead to the increase of SO_2 emission (Supplement Figure 5). The data from international energy association (IEA) reveals China has produced 3.7% more electricity from coal-based power plants in April 2020 than during April 2019 (IEA, 2020). The report by Global Energy Monitor (GEM, 2020) revealed China has increase its spending up to 14% in utilities, especially in power generation sector amidst the overall fall of capital spending by 6%. The same analysis further showed, in 2020, the total number of thermal-based power plant under development is 249.6 GW which is 21% higher than end of 2019 (205.9 GW). Such expansion of the coal-based thermal power plant, combining with the rebounding industrial demand after initial slow down due to lockdown measure (Jan–March), has led to surging of coal import up to 35% in April from a year earlier. The coal treaders also scrambled to low price due to plunging coal demand because of the outbreak of COVID-19. Such lower price also insists China to import more coal to fulfil its energy demand under current plan. As coal-burning is one of the prime sources of SO_2 emission, the emission of SO_2 from these coal-based thermal power plants has increased the optical depth by forming sulfate aerosols in the atmosphere under the presence of adequate moisture content and low wind speed (Supplement Figure 6 - 7). Our analysis further showed, at low humidity (preferably at 40–55% of RH) and low wind speed (below 3 m s^{-1}), the SO_2 concentration remains high (Fig. 8) which was observed in western, north-eastern and some of the areas in the east of China in SSEA region. The higher SO_2 concentration under a humidity level of 40–80% combining with low wind speed enhances the AOD that

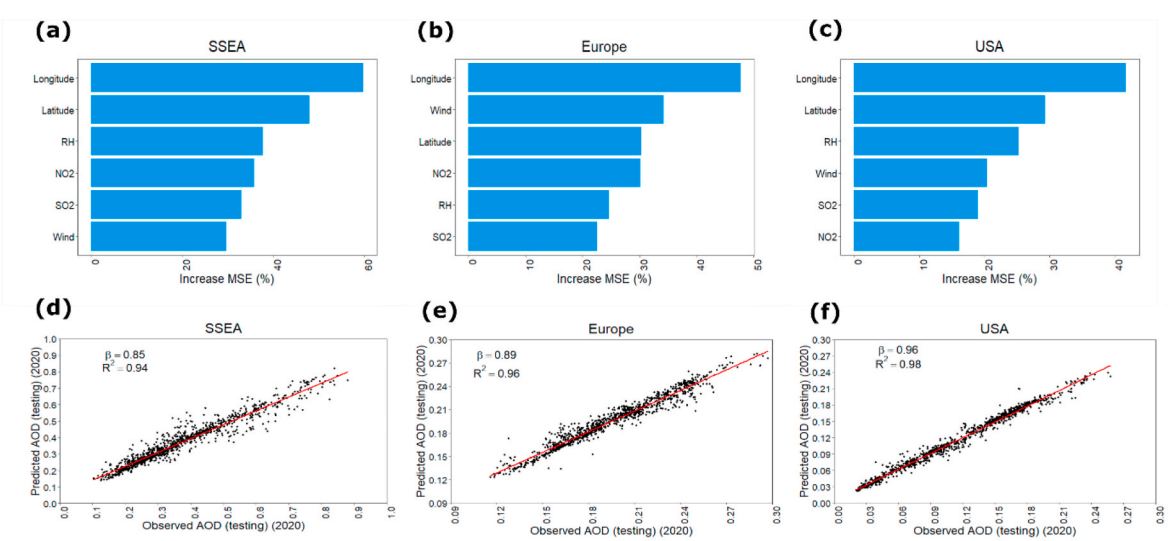

Fig. 5. The relative importance of the emission and meteorological parameters derived through the RF regression is shown in the first row. In the second row, the model performance (R^2) is demonstrated using the validation set of the sampled data.

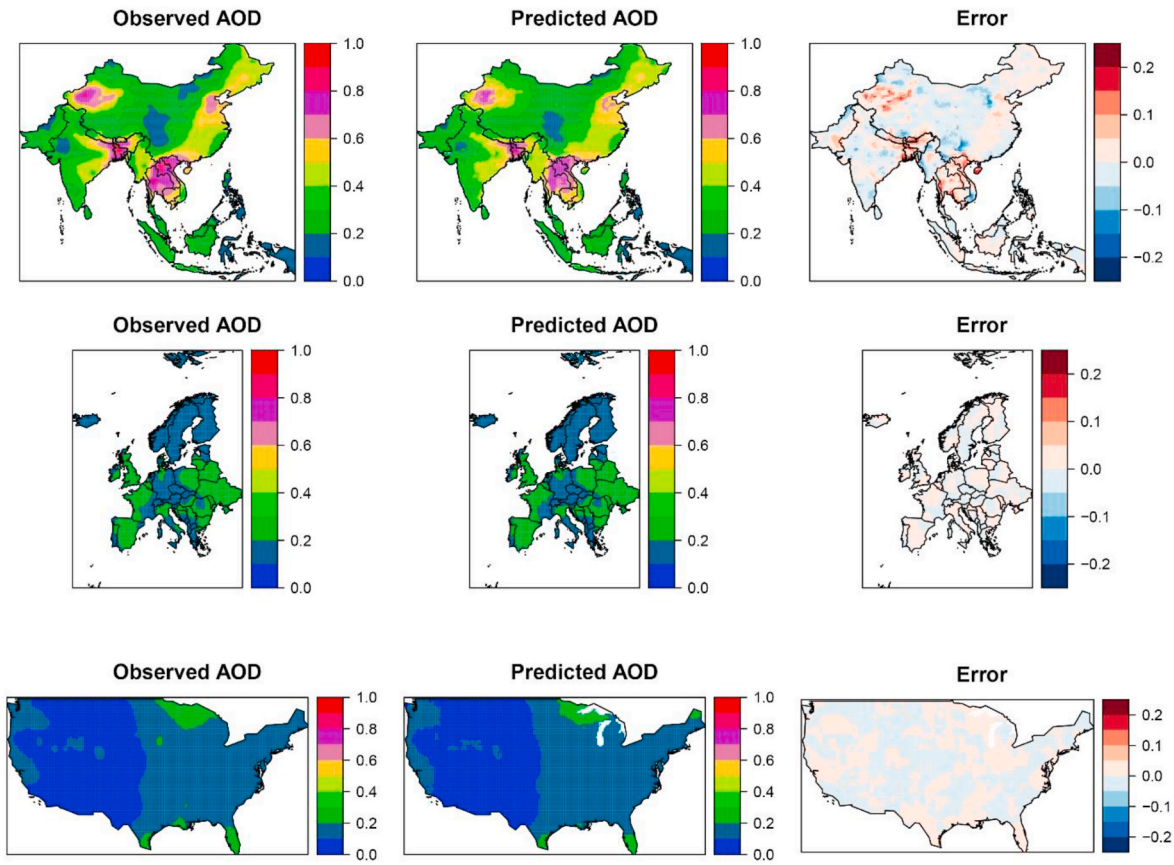

Fig. 6. The observed (the first column) and predicted AOD (second column), and estimation error (third column) of AOD - using RF regression-over SSEA, Europe and US regions during the lockdown period.

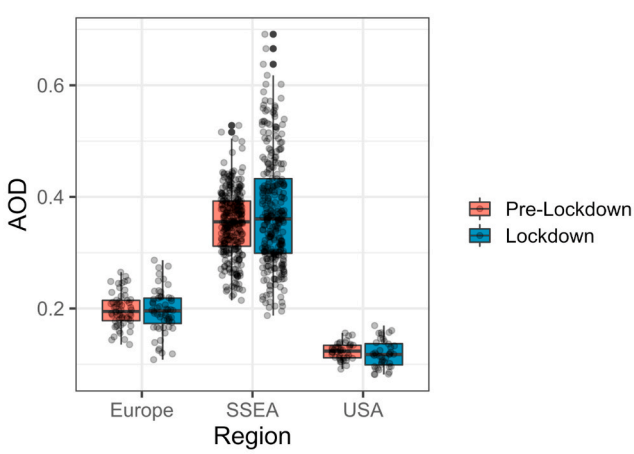

Fig. 7. The comparative boxplot showing average AOD over SSEA, Europe, and US regions during pre-lockdown and lockdown period.

is observed in the western, north-east and south-eastern Chinese territory. The western part of China which contains almost no population, the high AOD during the lockdown period is attributed to particulate matter emission from desert in this region, including the long-range transportation of pollutants from central Asia and eastern European portions through active wind system (Supplement Figure 8). The adherence of the molecules of sulfate and other suspended aqueous solutions on to the surface of these desert-dust form an external mixture that enhances the backscattering fraction of the incoming radiation resulting into high AOD (Seinfeld and Pandis, 2006; Pilinis et al., 1995). Furthermore, the spatial pattern of the vertical airflow at 850 hPa, analyzed using daily Reanalysis data during the lockdown period shows a positive omega, i.e. downward vertical flow (Supplement Figure 9a), was dominated in the western China resulting in to tapping of the pollutants within the boundary layer of the atmosphere, and thereby increase the AOD (Ogen, 2020).

The weekly anomaly of SO_2 suggests a significantly ($z_x > 1.96$) higher SO_2 concentration over the Tibetan high and its surroundings. Such higher positive anomaly over the Tibetan high is unusual, which could primarily be attributed to long-range transportation through the wind system (Han et al., 2019), including the downward vertical wind flow (Supplement Figure 9a). The back-trajectory analysis from NOAA-HYSPLIT model over this area showed the air masses originated over eastern Europe, middle-east and areas over India, Pakistan and Afghanistan (Supplement Figure 8). The higher positive-RPD of AOD over Thailand, Laos and Vietnam was, primarily, attributed to the vegetation fire that generally happens in this region at the beginning of summer season (Vadrevu et al., 2019; Mehta et al., 2016). The fire spots were detected in MODIS image during the seventh through ninth week (14th March – 14th April) of the period of lockdown (Supplement Figure 10) in this area. The consequent positive anomaly of NO_2 and SO_2 (Supplement Figure 3a, 4a) over this area implying their sources to the vegetation fire during the period mentioned above.

The higher positive-RPD of AOD in eastern India and Bangladesh during the lockdown period, considered for SSEA region, is attributed to the emissions from transport, energy and urban-industrial sources prior to the imposition of the lockdown measure in these countries. It was noted that, relative to the concentration of NO_2, a higher concentration of SO_2 (weekly SO_2 anomaly (z_x) > 0.5) prevailed in most of these areas much before the imposition of lockdown measures. As presented in Fig. 8, a relatively low amount of RH and low WS (Supplement Figure 6 -

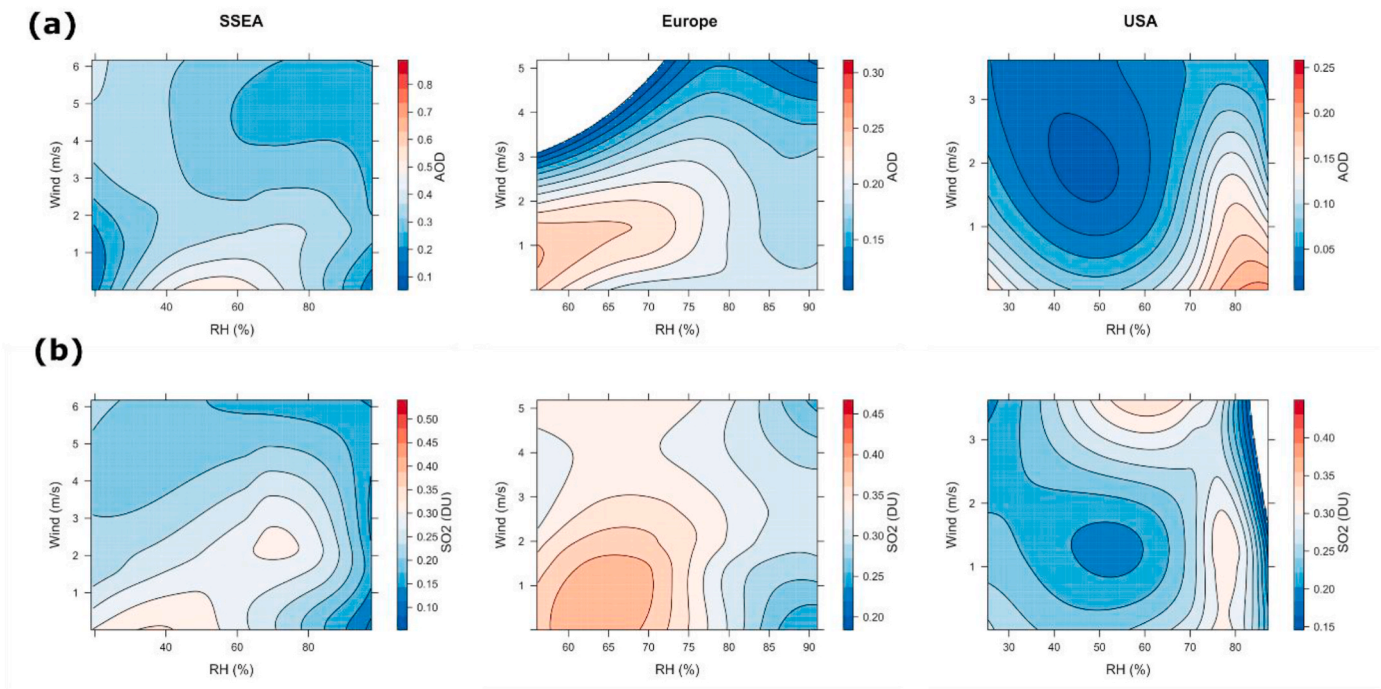

Fig. 8. (a) Interaction among relative humidity, wind speed and AOD, and (b) interaction among relative humidity, wind speed and SO_2 over SSEA, Europe and US regions during the lockdown period. The levelplots were prepared based on the sampling points ($n = 2500$) which were used to extract the values from the averages of AOD, RH, WS and SO_2 during the lockdown period (2020).

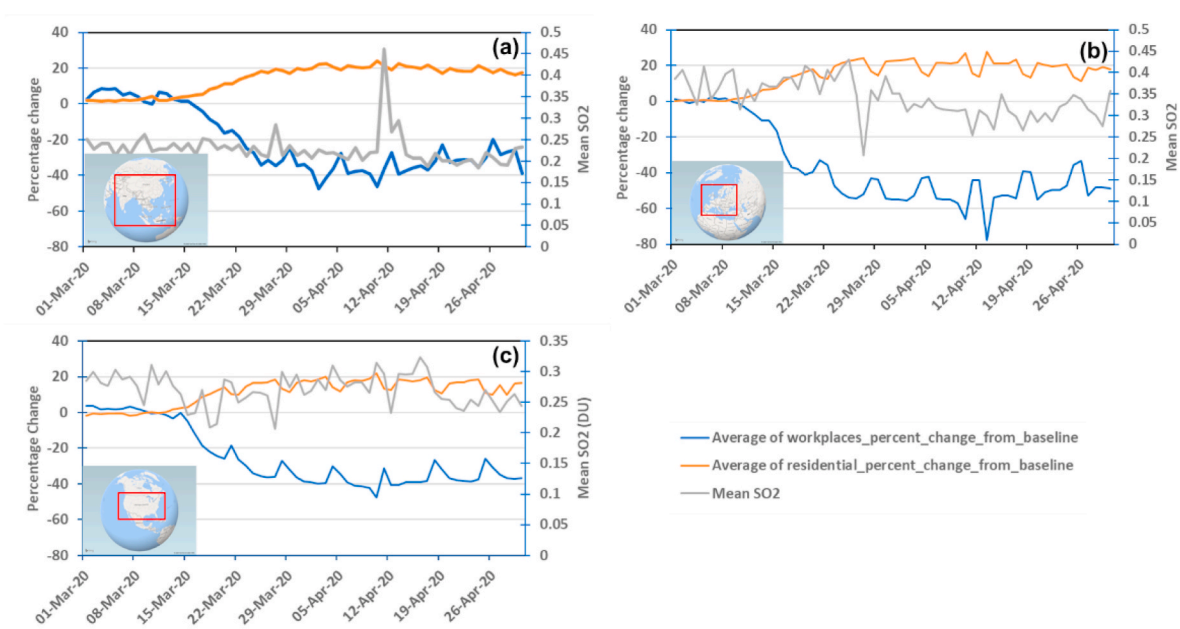

Fig. 9. Changes in the mobility of workplace and residential activities from their baseline. The mobility data was taken from Google mobility report (https://www.google.com/covid19/mobility/) during the lockdown period. The mobility report excludes the Chinese territory as there was no information on the mobility over China.

7) produce higher SO_2 concentration even under low amount of emission from the energy sector, especially the thermal power plants. The weekly AOD anomaly over India, however, showed a significant decrease in the Indo-Gangetic plain (IGP), especially in the north-west part of it at the beginning of lockdown. Mahato et al. (2020) reported the reduction of PM_{10} and $PM_{2.5}$ up to 51.8% and 53.1% over the national capital region (NCR) of India, Delhi. The same study also claimed a reduction of NO_2 concentration up to 52.6% in the first three weeks of lockdown, while SO_2 reduced up to 18% over Delhi-NCR. The report relating to the Google mobility index over India manifested a reduction of 85% retail and recreation, and 64% transportation activity (Google LLC, 2020). Such a reduction in the economic activities by the law enforcement had significantly decreased the NO_2 emissions resulting in low aerosol load. The apparent difference in the changes of aerosol load in the western and eastern part of the IGP could further be attributed to the unusual frequency of precipitation in this year in the western IGP through western disturbance (IMD, 2020). Additionally, the mining areas in eastern India were in the operational mode and emit a high

amount of particulate matter that escalate optical depth in these areas during the lockdown period (Ranjan et al., 2020). The RPD of relative humidity over the SSEA region showed an overall increase. However, average RH during the lockdown period was more than 80% for most of the areas over China, while it was less than 50% in areas over India, Pakistan and Bangladesh. The high ambient relative humidity combined with higher wind speed helped to reduce aerosol concentration in the atmosphere through accentuating aggregation of primary aerosol particles (Fig. 8a). In contrasts, under the presence of precursor gases such as SO_2, such high ambient RH forms secondary aerosol particles leading to the increase of AOD (Fig. 8b). The weekly variation of AOD-anomaly, thus, closely related to the complex interaction of the source strength of the emission of particulate and gaseous maters and their removal process through relative humidity and wind action. For other areas of SSEA region such as Myanmar, Thailand, Laos, Cambodia, Indonesia, Malaysia, Vietnam etc. in the south-east, where lockdown measures were imposed at different points of time, the weekly variation in AOD during the period of lockdown is governed by this process of complex interaction, including the outbreak of fire events.

By an estimate over Europe, the reduction of emissions was measured up to 89%, 86%, 82% 47% and 70% from transport sectors in Spain, Italy, France, Germany and UK, respectively (Muhammad et al., 2020). We, however, estimated a reduction of NO_2 up to 20–40% in those countries, excluding Spain. The high RPD values (up to 60% increase) of AOD during lockdown period over western Europe, especially over Spain and Portugal, is primarily attributed to the emission from power plants which used a range of different forms of fuel such as coal, oil, natural gas, biomass and combustible waste materials (Supplement Figure 5). The source-based energy production for the month of April for countries in Europe showed a majority of the countries switched over to the biomass and combustible waste for producing power to meet the escalated domestic energy demand, yet, the total energy production has reduced substantially due to reduction in industrial activity (IEA, 2020). An estimation showed that coal-based energy production had reduced more than 30% due to reduction in coal production because of COVID-19 (IEA, 2020), while biomass and other combustible waste-based energy production has increased more than 20%. The weekly anomaly of SO_2 over western Europe, consisting of Spain, Portugal, and France, evidenced a high positive anomaly. A similar magnitude of SO_2 anomaly is also observed in other south-east European countries where a higher positive RPD of RH is also obtained (Supplement Figure 6). As mentioned earlier, such a higher amount of moisture content combining with the low wind speed act as a catalyst to increase the optical depth by forming new particles (Fig. 8). In conjunction with low wind speed and a higher moisture content, the spatial pattern of vertical air flow reveals a high magnitude of positive omega (at 850 hPa) for western European countries (Ogen, 2020), such as Spain, Portugal, France, southern England, the countries in the southern Europe and south-east Europe (Supplement Figure 9b), which is closely matching with the spatial pattern of positive RPD for AOD and SO_2 concentration. Such downward wind flow restricts the ventilation of the emitted pollutant and keep them within the boundary layer of the lower troposphere causing high AOD during lockdown period. Additionally, the 7-days back-trajectory analysis showed evidence of long-range transportation of gaseous pollutants from the areas over eastern Europe to this part of western Europe (Supplement Figure 11). The weekly anomalies of NO_2 and SO_2 indeed showed a time-space variation of these pollutants with a variation of stern economic restrictions.

Like SSEA and European region, the US also showed a significant reduction of NO_2 due to lockdown measures. In contrast, the higher RPD and weekly positive anomaly of SO_2 indicated to the emission from power plants that remained operational during the lockdown period. The energy statistics from IEA over the US showed a reduction of electricity production by an amount of 31.9% using coal. However, the production of electricity from oil and combustible waste materials has increased by 7.5% and 16.6%, respectively (IEA, 2020). The moisture change – from pre-lockdown to lockdown period - for the majority of areas over the US remained within ±10% (Supplement Figure 6). The south-west part of the USA showed a relatively higher amount of positive change of RH though mean relative humidity in this region ranges from 30 to 60%. The interaction of SO_2, RH and wind speed, for the US region, showed that under the controlled emission, when SO_2 remains under 0.25 DU, 30–60% of RH in combination with the WS, greater than 2 m s^{-1}, lowers the AOD (Fig. 8). In contrasts, 0.30–0.35 DU of SO_2 concentration combining with a higher relative humidity (>80%) and a wind speed below 2 m s^{-1} increase the AOD for US region. In conjunction with the complex interaction of meteorological and emission factors, the apparent difference of AOD in the eastern and western US is attributed to the spatial variation of vertical wind velocity (Supplement Figure 9c), including the variation of urban-industrial density that emits a distinct quantity of primary aerosols and trace gases leading to a notable difference in the magnitude of AOD. We also looked into the complex relationship of meteorology and SO_2 during the pre-lockdown period for all three regions to understand their distinguishable effect on the occurrence of AOD from the lockdown period (Supplement Figure 12a). The analysis, however, does not reveal any important changes in their relationship, at least for SSEA and USA. However, certain degree of variation in this relationship for pre-lockdown period is observed for European region. Low WS (≤1 m s^{-1}) and high RH (>75%) is associated with high SO_2 concentration (Supplement Figure 12b). This high SO_2 concentration is a result of the combined emission from industrial and energy sectors under such meteorological state, and thereby producing a high AOD. In contrasts to the status of this relationship during the lockdown period, high magnitude of AOD is observed over Europe during pre-lockdown period (Supplement Figure 12a) despite low SO_2 concentration under relatively high WS (>1 m s^{-1}) and less than 70% of RH. Such relationship among these variables implying to the long-range wind transportation of the pollutants that increase the AOD.

Service and Industrial sectors (office, education, hospitality, retail, tourism, etc.) were almost entirely closed in many countries due to COVID-19 situation. Therefore, the electricity demand of the service and industrial sector had been reduced, while the domestic/residential electricity demand increased as a significant number of individuals were spending more time at home and are working through teleworking mode. The industrial-electricity demand, however, may not drop significantly for many regions, as many essential industries were able to continue their regular production with precautionary measures. Therefore, total power demand might have decreased but was not radically fallen specifically in the developed countries where people engaged in teleworking mode. The analysis of the changes in human mobility from Google mobility report (Google LLC, 2020) demonstrated that lockdown has significantly reduced workplace mobility and increased residential mobility up to 20–40%. Over the SSEA region (excluding China, as no information in mobility was available for China), no profound effect of the reduction of workplace mobility and increase of residential mobility was observed on the SO_2 emission (Fig. 9a). In contrast, in the US, the SO_2 curve is closely matching with the increase in residential mobility during the lockdown period and thereby causing a significant positive relationship ($r = 0.37$, p-value = 0.01). Such an association indicates the emission from the power sector due to escalated demand for staying in and working from home (Fig. 9c). In Europe, the SO_2 curve followed the residential mobility curve for the first two weeks of the lockdown measure in March. After that, the SO_2 decreased due to further reduction of urban-industrial activities in combination with the complex interaction of RH and WS; however, its fluctuations nearly matched the residential mobility curve (Fig. 9b). As the SSEA region is having a wide spectrum of developing and underdeveloped nations whose energy usage quantities are significantly different from the developed group of nations, the home staying did not considerably influence to the rise the SO_2 concentration in SSEA region during the lockdown period. The emission from local sources in combination with cropland and forest

fires, had instead increased the SO_2 concentration in this region.

The RF regression manifested distinguishable response of the input variables in three regions. For the SSEA region, the variation of RH and the emission characteristics (i.e. NO_2 and SO_2) plays an important role in causing spatial variation of AOD during the lockdown period. Over the US region, it's the meteorological factors and SO_2 that play important role, while for the European region, the meteorological field, i.e. wind speed, and the NO_2 emission play crucial role in causing spatial variation of AOD. It is noteworthy that the contribution of geolocation fields, especially the longitude, amongst all selected variables, contribute significantly higher in explaining the spatial variation of AOD. Due to a large variety of physiographic and climatic conditions, in combination with a considerable variation of urban-industrial activity that spits various magnitudes of gaseous and particulate matters, the geolocation fields have the strongest influence in causing spatial variation of AOD for SSEA and USA regions.

6. Conclusions

In summary, the results demonstrated a significant decrease in AOD over densely populated regions. A substantial reduction in NO_2 emission was obtained due to imposition of lockdown measures in most of the areas over SSEA, Europe and the US. Our results demonstrated a higher SO_2 emission for the majority of areas in these regions during the lockdown period. The discrepancy in the concentrations of NO_2 and SO_2 suggests to the restriction in traffic movement - considered as one of the prime sources of NO_2 emission - leading to reduction in NO_2 concentration. In contrast, increase in SO_2 during the lockdown period was related to the emission from the power plants due to existing energy demand because of home staying and working from home to contain the spread of the virus, including the industrial energy demand that somewhat lower than the pre-lockdown period. Additionally, the complex interaction of wind speed and ambient relative humidity with the emitted SO_2 plays an essential role in causing spatial variation of SO_2.

The relative changes in AOD, NO_2 and SO_2 during the lockdown period in comparison to their pre-lockdown state appeared statistically significant, implying the role of causative measures to reduce the aerosol load. The results also pointed out the formation of new particles from the emitted SO_2 under high RH and low WS that is in line with the theoretical underpinnings of secondary aerosol particle formation in the atmosphere. The findings included clear inter week variation of the AOD, NO_2, and SO_2 anomaly during lockdown period. Such variations are essential to understand the progress of lockdown measures which were imposed by the respective countries and provinces in these regions at different points of time. Withstanding such regional variation of lockdown measures, the findings also acknowledge the incumbent role of the mesoscale variation of wind speed and atmospheric moisture fields in causing spatial variation of AOD during the lockdown period. The RF regression model indicated a distinguishable influence pattern of the meteorological and emission factors among the SSEA, Europe and US regions. As the lockdown measures were applied at various intensities, the RH and emission characteristic, especially the concentration of NO_2, are more important in causing spatial variation of AOD in SSEA region. In contrast, the WS, RH and the emission of SO_2, are more critical in creating the spatial variation of AOD for the US region.

The mean values of aerosol loading during the pre-lockdown period, as found in the results, were distinguishable for Europe and the US regions as compared to the SSEA region. Excluding the natural dust and biomass burning aerosols, that primarily come from the occurrence of a vegetation fire, the low AOD level in Europe and the US is due to the strongest implication of the emission policies for the industrial, domestic and transport sector emission. The lockdown measures, however, evidenced a significant reduction of the aerosol load over major urban-industrial regions in SSEA, especially, over India and China. The reports concerning the improvement in the visibility in different parts of India and China showcased how important the anthropogenic emissions were in lowering the ambient air quality. Despite low mean aerosol load, the air quality also improved over major urban-industrial clusters in the US and Europe due to effective lockdown measures. The results also showcased significant association of escalated power demand and SO_2 emission at least for the US, yet, such linkage was weak for SSEA region.

Based on the evidences presented, the findings of this study acknowledged the effect of reduced emission in lowering the aerosol load and cleaning of the ambient air at a continental scale, and suggest the need for switching over to the cleaner mode of production, fuel use and energy usage in combating with the persistent air quality issue. The worldwide spread of the COVID-19 and the consequent global economic shut down has opened up a discourse for the real-time experiment of a new regime of anthropogenic emissions on global aerosol load and thereby responding to the need of using clean energy, or framing alternative energy policy for a better environment.

Credit author statement

Prasenjit Acharya, conceptualized the work and drafted the manuscript. Gunadhar Barik, Bijoy Krishna Gayen, Somnath Bar, Arabinda Maiti and Ashis Sarkar, Formal analysis. Surajit Ghosh, Sikhendra Kisor De and S Sreekesh, contributed to the improvement of the draft manuscript.

Declaration of competing interest

The authors declare that they have no known competing financial interests or personal relationships that could have appeared to influence the work reported in this paper.

Acknowledgements

The authors acknowledged the support from Giovanni online data system, developed and maintained by the NASA GES DISC, for archiving the daily atmospheric data - essential for the analysis. We also extend our thanks to NOAA/OAR/ESRL PSL, Boulder, Colorado, USA, for providing analysis-ready NCEP Reanalysis data of relative humidity. We are thankful to the University Grants Commission, Government of India, for supporting research activities under fellowship number UGC-Ref. No. 3231(NET-JUNE2015), UGC-Ref. No. 3289/(SC) (NET-JAN2017) and UGC-Ref. No. 3524/(NET-JULY2018). The authors also acknowledge the Department of Science and Technology, Government of India, for proving fund (SR/FST/SR/FST/ES-I/2017/7/2017) to the Department of Geography, Vidyasagar University, for improving skills of teaching and research. We also extend our gratitude to the two anonymous reviewers for making significant comments towards improving the quality of the manuscript.

Appendix A. Supplementary data

Supplementary data to this article can be found online at https://doi.org/10.1016/j.envres.2020.110514.

References

Abdullah, S., Mansor, A.A., Napi, N.N.L.M., Mansor, W.N.W., Ahmed, A.N., Ismail, M., Ramly, Z.T.A., 2020. Air quality status during 2020 Malaysia Movement Control Order (MCO) due to 2019 novel coronavirus (2019-nCoV) pandemic. Sci. Total Environ. https://doi.org/10.1016/J.SCITOTENV.2020.139022.

Bao, R., Zhang, A., 2020. Does lockdown reduce air pollution?: evidence from 44 cities in northern China. Sci. Total Environ. https://doi.org/10.1016/J.SCITOTENV.2020.139052.

Bhartia, P.K., 2002. OMI Algorithm Theoretical Basis Document. NASA-OMI, Washington, DC. ATBD-OMI-02, version 2.0 II, 1–91.

Breiman, L., 2001. Random forests. Mach. Learn. 45, 5–32. https://doi.org/10.1201/9780367816377-11.

Broomandi, P., Karaca, F., Nikfal, A., Jahanbakshi, A., Tamjidi, M., Kim, J.R., 2020. Impact of the COVID-19 event on the air quality in Iran. Aerosol Air Qual. Res. 20, 915–929. https://doi.org/10.4209/aaqr.2020.04.0150.

Bucsela, E.J., Krotkov, N.A., Celarier, E.A., Lamsal, L.N., Swartz, W.H., Bhartia, P.K., Boersma, K.F., Veefkind, J.P., Gleason, J.F., Pickering, K.E., 2013. A new stratospheric and tropospheric NO2 retrieval algorithm for nadir-viewing satellite instruments: applications to OMI. Atmos. Meas. Tech. 6, 2607–2626. https://doi.org/10.5194/amt-6-2607-2013.

Chauhan, A., Singh, R.P., 2020. Decline in PM2.5 concentrations over major cities around the world associated with COVID-19. Environ. Res. 187, 109634. https://doi.org/10.1016/j.envres.2020.109634.

Chin, M., Diehl, T., Tan, Q., Prospero, J.M., Kahn, R.A., Remer, L.A., Yu, H., Sayer, A.M., Bian, H., Geogdzhayev, I.V., Holben, B.N., Howell, S.G., Huebert, B.J., Hsu, N.C., Kim, D., Kucsera, T.L., Levy, R.C., Mishchenko, M.I., Pan, X., Quinn, P.K., Schuster, G.L., Streets, D.G., Strode, S.A., Torres, O., 2014. Multi-decadal aerosol variations from 1980 to 2009: a perspective from observations and a global model. Atmos. Chem. Phys. 14, 3657–3690. https://doi.org/10.5194/acp-14-3657-2014.

Cohen, A.J., Brauer, M., Burnett, R., Anderson, H.R., Frostad, J., Estep, K., Balakrishnan, K., Brunekreef, B., Dandona, L., Dandona, R., Feigin, V., Freedman, G., Hubbell, B., Jobling, A., Kan, H., Knibbs, L., Liu, Y., Martin, R., Morawska, L., Pope, C.A., Shin, H., Straif, K., Shaddick, G., Thomas, M., van Dingenen, R., van Donkelaar, A., Vos, T., Murray, C.J.L., Forouzanfar, M.H., 2017. Estimates and 25-year trends of the global burden of disease attributable to ambient air pollution: an analysis of data from the Global Burden of Diseases Study 2015. Lancet 389, 1907–1918. https://doi.org/10.1016/S0140-6736(17)30505-6.

Collivignarelli, M.C., Abbà, A., Bertanza, G., Pedrazzani, R., Ricciardi, P., Carnevale Miino, M., 2020. Lockdown for CoViD-2019 in Milan: what are the effects on air quality? Sci. Total Environ. 732, 139280. https://doi.org/10.1016/j.scitotenv.2020.139280.

Crippa, M., Solazzo, E., Huang, G., Guizzardi, D., Koffi, E., Muntean, M., Schieberle, C., Friedrich, R., Janssens-Maenhout, G., 2020. High resolution temporal profiles in the emissions database for global atmospheric research. Sci. Data 7, 1–17. https://doi.org/10.1038/s41597-020-0462-2.

Dantas, G., Siciliano, B., Franca, B.B., Silva, C.M.D., Arbilla, G., 2020. The impact of COVID-19 partial lockdown on the air quality of the city of Rio de Janeiro, Brazil. Sci. Total Environ. https://doi.org/10.1016/J.SCITOTENV.2020.139085.

Draxler, R.R., Hess, G.D., G, D., 1998. An overview of the HYSPLIT_4 modeling system of trajectories, dispersion, and deposition. Aust. Meteorol. Mag. 47, 295–308.

Fioletov, V.E., McLinden, C.A., Krotkov, N., Li, C., Joiner, J., Theys, N., Carn, S., Moran, M.D., 2016. A global catalogue of large SO2 sources and emissions derived from the Ozone Monitoring Instrument. Atmos. Chem. Phys. 16, 11497–11519. https://doi.org/10.5194/acp-16-11497-2016.

GEM, 2020. A New Coal Boom in China - Global Energy Monitor. https://globalenergymonitor.org/wp-content/uploads/2020/06/China-coal-plant-brief-June-2020v2.pdf. (Accessed 23 October 2020).

Glantz, P., Freud, E., Johansson, C., Noone, K.J., Tesche, M., 2019. Trends in MODIS and AERONET derived aerosol optical thickness over Northern Europe. Tellus Ser. B Chem. Phys. Meteorol. 71, 1–21. https://doi.org/10.1080/16000889.2018.1554414.

Google LLC, 2020. Google COVID-19 Community Mobility Reports. Google. https://www.google.com/covid19/mobility/. (Accessed 17 June 2020).

Gupta, P., Remer, L.A., Levy, R.C., Mattoo, S., 2018. Validation of MODIS 3km land aerosol optical depth from NASA's EOS Terra and Aqua missions. Atmos. Meas. Tech. 11, 3145–3159. https://doi.org/10.5194/amt-11-3145-2018.

Han, B., Wang, J., Zhao, X., Yin, B., Wang, X., Dou, X., Yang, W., Bai, Z., 2019. Characterizations and source analysis of atmospheric inorganic ions at a national background site in the northeastern Qinghai-Tibet Plateau: insights into the influence of anthropogenic emissions on a high-altitude area of China. Atmos. Chem. Phys. Discuss. 1–26. https://doi.org/10.5194/acp-2018-1345.

He, L., Zhang, S., Hu, J., Li, Z., Zheng, X., Cao, Y., Xu, G., Yan, M., Wu, Y., 2020. On-road emission measurements of reactive nitrogen compounds from heavy-duty diesel trucks in China. Environ. Pollut. 262 https://doi.org/10.1016/j.envpol.2020.114280.

He, M.Z., Kinney, P.L., Li, T., Chen, C., Sun, Q., Ban, J., Wang, J., Liu, S., Goldsmith, J., Kioumourtzoglou, M.A., 2020. Short- and intermediate-term exposure to NO2 and mortality: a multi-county analysis in China. Environ. Pollut. 261, 114165. https://doi.org/10.1016/j.envpol.2020.114165.

Hilboll, A., Richter, A., Burrows, J.P., 2013. Long-term changes of tropospheric NO2 over megacities derived from multiple satellite instruments. Atmos. Chem. Phys. 13, 4145–4169. https://doi.org/10.5194/acp-13-4145-2013.

Hsu, N.C., Jeong, M.J., Bettenhausen, C., Sayer, A.M., Hansell, R., Seftor, C.S., Huang, J., Tsay, S.C., 2013. Enhanced Deep Blue aerosol retrieval algorithm: the second generation. J. Geophys. Res. Atmos. 118, 9296–9315. https://doi.org/10.1002/jgrd.50712.

IEA, 2020. Monthly Electricity Statistics. IEA, Paris, 17th August. 2020. https://www.iea.org/reports/monthly-electricity-statistics.

Irie, H., Boersma, K.F., Kanaya, Y., Takashima, H., Pan, X., Wang, Z.F., 2012. Quantitative bias estimates for tropospheric NO2 columns retrieved from SCIAMACHY, OMI, and GOME-2 using a common standard for East Asia. Atmos. Meas. Tech. 5, 2403–2411. https://doi.org/10.5194/amt-5-2403-2012.

Jing-Mei, Y., Jin-Huan, Q., Yan-Liang, Z., 2010. Validation of aerosol optical depth from Terra and aqua MODIS retrievals over a tropical coastal site in China. Atmos. Oceanogr. Sci. Libr. 3, 36–39. https://doi.org/10.1080/16742834.2010.11446834.

Kalnay, E., Kanamitsu, M., Kistler, R., Collins, W., Deaven, D., Gandin, L., Iredell, M., Saha, S., White, G., Woollen, J., Zhu, Y., Chelliah, M., Ebisuzaki, W., Higgins, W., Janowiak, J., Mo, K.C., Ropelewski, C., Wang, J., Leetmaa, A., Reynolds, R., Jenne, R., Joseph, D., 1996. The NCEP/NCAR 40-year reanalysis project. Bull. Am. Meteorol. Soc. https://doi.org/10.1175/1520-0477(1996)077<0437:TNYRP>2.0.CO, 2.

Kanniah, K.D., Kamarul Zaman, N.A.F., Kaskaoutis, D.G., Latif, M.T., 2020. COVID-19's impact on the atmospheric environment in the Southeast Asia region. Sci. Total Environ. 736, 139658. https://doi.org/10.1016/j.scitotenv.2020.139658.

Klimont, Z., Kupiainen, K., Heyes, C., Purohit, P., Cofala, J., Rafaj, P., Borken-Kleefeld, J., Schöpp, W., 2017. Global anthropogenic emissions of particulate matter including black carbon. Atmos. Chem. Phys. 17, 8681–8723. https://doi.org/10.5194/acp-17-8681-2017.

Krotkov, N.A., McLinden, C.A., Li, C., Lamsal, L.N., Celarier, E.A., Marchenko, S.V., Swartz, W.H., Bucsela, E.J., Joiner, J., Duncan, B.N., Folkert Boersma, K., Pepijn Veefkind, J., Levelt, P.F., Fioletov, V.E., Dickerson, R.R., He, H., Lu, Z., Streets, D.G., 2016. Aura OMI observations of regional SO2 and NO2 pollution changes from 2005 to 2015. Atmos. Chem. Phys. 16, 4605–4629. https://doi.org/10.5194/acp-16-4605-2016.

Lamsal, L.N., Martin, R.V., Van Donkelaar, A., Celarier, E.A., Bucsela, E.J., Boersma, K.F., Dirksen, R., Luo, C., Wang, Y., 2010. Indirect validation of tropospheric nitrogen dioxide retrieved from the OMI satellite instrument: insight into the seasonal variation of nitrogen oxides at northern midlatitudes. J. Geophys. Res. Atmos. 115, 1–15. https://doi.org/10.1029/2009JD013351.

Levy, R.C., Remer, L.A., Kleidman, R.G., Mattoo, S., Ichoku, C., Kahn, R., Eck, T.F., 2010. Global evaluation of the Collection 5 MODIS dark-target aerosol products over land. Atmos. Chem. Phys. 10, 10399–10420. https://doi.org/10.5194/acp-10-10399-2010, 2010.

Levy, R.C., Mattoo, S., Munchak, L.A., Remer, L.A., Sayer, A.M., Patadia, F., Hsu, N.C., 2013. The Collection 6 MODIS aerosol products over land and ocean. Atmos. Meas. Tech. 6, 2989–3034. https://doi.org/10.5194/amt-6-2989-2013.

Li, C., Joiner, J., Krotkov, N.A., Bhartia, P.K., 2013. A fast and sensitive new satellite SO2 retrieval algorithm based on principal component analysis: application to the ozone monitoring instrument. Geophys. Res. Lett. 40, 6314–6318. https://doi.org/10.1002/2013GL058134.

Mahato, S., Pal, S., Ghosh, K.G., 2020. Effect of lockdown amid COVID-19 pandemic on air quality of the megacity Delhi, India. Sci. Total Environ. 730, 139086. https://doi.org/10.1016/j.scitotenv.2020.139086.

Mehta, M., Singh, R., Singh, A., Singh, N., Anshumali, 2016. Recent global aerosol optical depth variations and trends - a comparative study using MODIS and MISR level 3 datasets. Remote Sens. Environ. 181, 137–150. https://doi.org/10.1016/j.rse.2016.04.004.

Misra, A., Jayaraman, A., Ganguly, D., 2008. Validation of MODIS derived aerosol optical depth over Western India. J. Geophys. Res. Atmos. 113, 1–12. https://doi.org/10.1029/2007JD009075.

Muhammad, S., Long, X., Salman, M., 2020. COVID-19 pandemic and environmental pollution: a blessing in disguise? Sci. Total Environ. 728, 138820. https://doi.org/10.1016/j.scitotenv.2020.138820.

Nakada, L.Y.K., Urban, R.C., 2020. COVID-19 pandemic: impacts on the air quality during the partial lockdown in São Paulo state. Brazil. Sci. Total Environ. 730, 139087. https://doi.org/10.1016/j.scitotenv.2020.139087.

Ogen, Y., 2020. Assessing nitrogen dioxide (NO2) levels as a contributing factor to coronavirus (COVID-19) fatality. Sci. Total Environ. 726, 138605. https://doi.org/10.1016/j.scitotenv.2020.138605.

Pilinis, C., Pandis, S.N., Seinfeld, J.H., 1995. Sensitivity of direct climate forcing by atmospheric aerosols to aerosol size and composition. J. Geophys. Res. 100, 18739. https://doi.org/10.1029/95JD02119.

Ranjan, A.K., Patra, A.K., Gorai, A.K., 2020. Effect of lockdown due to SARS COVID-19 on aerosol optical depth (AOD) over urban and mining regions in India. Sci. Total Environ. 745, 141024. https://doi.org/10.1016/j.scitotenv.2020.141024.

Remer, L.A., Kleidman, R.G., Levy, R.C., Kaufman, Y.J., Tanré, D., Mattoo, S., Martins, J. V., Ichoku, C., Koren, I., Yu, H., Holben, B.N., 2008. Global aerosol climatology from the MODIS satellite sensors. D14S07 J. Geophys. Res. Atmos. 113. https://doi.org/10.1029/2007JD009661, 2008.

Remer, L.A., Kaufman, Y.J., Tanré, D., Mattoo, S., Chu, D.A., Martins, J.V., Li, R.-R., Ichoku, C., Levy, R.C., Kleidman, R.G., Eck, T.F., Vermote, E., Holben, B.N., 2005. The MODIS aerosol algorithm, products, and validation. J. Atmos. Sci. 62, 947–973. https://doi.org/10.1175/JAS3385.1.

Seinfeld, J., Pandis, S., 2006. Atmospheric Chemistry and Physics, second ed. John Wiley & Sons, Inc., New Jersy.

Sharma, S., Zhang, M., Anshika Gao, J., Zhang, H., Kota, S.H., 2020. Effect of restricted emissions during COVID-19 on air quality in India. Sci. Total Environ. 728, 138878. https://doi.org/10.1016/j.scitotenv.2020.138878.

Sicard, P., De Marco, A., Agathokleous, E., Feng, Z., Xu, X., Paoletti, E., Rodriguez, J.J.D., Calatayud, V., 2020. Amplified ozone pollution in cities during the COVID-19 lockdown. Sci. Total Environ. 735, 139542. https://doi.org/10.1016/j.scitotenv.2020.139542.

Smith, S.J., Pitchera, H., Wigley, T.M.L., 2001. Global and regional anthropogenic sulfur dioxide emissions. Global Planet. Change 29, 99–119. https://doi.org/10.1016/S0921-8181(00)00057-6.

Smith, S.J., Van Aardenne, J., Klimont, Z., Andres, R.J., Volke, A., Delgado Arias, S., 2011. Anthropogenic sulfur dioxide emissions: 1850-2005. Atmos. Chem. Phys. 11, 1101–1116. https://doi.org/10.5194/acp-11-1101-2011.

Streets, D.G., Bond, T.C., Carmichael, G.R., Fernandes, S.D., Fu, Q., He, D., Klimont, Z., Nelson, S.M., Tsai, N.Y., Wang, M.Q., Woo, J.H., Yarber, K.F., 2003. An inventory of gaseous and primary aerosol emissions in Asia in the year 2000. J. Geophys. Res. Atmos. 108 https://doi.org/10.1029/2002jd003093.

Streets, D.G., Wu, Y., Chin, M., 2006. Two-decadal aerosol trends as a likely explanation of the global dimming/brightening transition. Geophys. Res. Lett. 33, 2–5. https://doi.org/10.1029/2006GL026471.

Tobías, A., Carnerero, C., Reche, C., Massagué, J., Via, M., Minguillón, M.C., Alastuey, A., Querol, X., 2020. Changes in air quality during the lockdown in Barcelona (Spain)

one month into the SARS-CoV-2 epidemic. Sci. Total Environ. 726, 138540. https://doi.org/10.1016/j.scitotenv.2020.138540.

Vadrevu, K.P., Lasko, K., Giglio, L., Schroeder, W., Biswas, S., Justice, C., 2019. Trends in vegetation fires in south and southeast asian countries. Sci. Rep. 9, 1–13. https://doi.org/10.1038/s41598-019-43940-x.

Wang, Pengfei, Chen, K., Zhu, S., Wang, Peng, Zhang, H., 2020. Severe air pollution events not avoided by reduced anthropogenic activities during COVID-19 outbreak. Resour. Conserv. Recycl. 158, 104814. https://doi.org/10.1016/j.resconrec.2020.104814.

Wei, J., Li, Z., Peng, Y., Sun, L., 2019. MODIS Collection 6.1 aerosol optical depth products over land and ocean: validation and comparison. Atmos. Environ. 201, 428–440. https://doi.org/10.1016/j.atmosenv.2018.12.004.

WHO, 2020. Advice for public. WHO. https://www.who.int/emergencies/diseases/novel-coronavirus-2019/advice-for-public. (Accessed 16 June 2020).

Yoon, J., Burrows, J.P., Vountas, M., Von Hoyningen-Huene, W., Chang, D.Y., Richter, A., Hilboll, A., 2014. Changes in atmospheric aerosol loading retrieved from space-based measurements during the past decade. Atmos. Chem. Phys. 14, 6881–6902. https://doi.org/10.5194/acp-14-6881-2014.

Yoon, J., Von Hoyningen-Huene, W., Kokhanovsky, A.A., Vountas, M., Burrows, J.P., 2012. Trend analysis of aerosol optical thickness and ngström exponent derived from the global AERONET spectral observations. Atmos. Meas. Tech. 5, 1271–1299. https://doi.org/10.5194/amt-5-1271-2012.

Yoon, J., Von Hoyningen-Huene, W., Vountas, M., Burrows, J.P., 2011. Analysis of linear long-term trend of aerosol optical thickness derived from SeaWiFS using BAER over Europe and South China. Atmos. Chem. Phys. 11, 12149–12167. https://doi.org/10.5194/acp-11-12149-2011.

Zhang, R., Zhang, Y., Lin, H., Feng, X., Fu, T.M., Wang, Y., 2020. NOx emission reduction and recovery during COVID-19 in East China. Atmosphere 11, 1–16. https://doi.org/10.3390/ATMOS11040433.

Zhao, T.X.P., Laszlo, I., Guo, W., Heidinger, A., Cao, C., Jelenak, A., Tarpley, D., Sullivan, J., 2008. Study of long-term trend in aerosol optical thickness observed from operational AVHRR satellite instrument. J. Geophys. Res. Atmos. 113, 1–14. https://doi.org/10.1029/2007JD009061.

IMD, 2020. Standardize Precipitation Index. http://www.imdpune.gov.in/hydrology/slider.html. Accessed 13th June. 2020.